Research Article

Chenghang Li, Zhumei Luo*, Shan Qing*, Haoming Huang, and Xiaohui Zhang

Differential study on the thermal–physical properties of metal and its oxide nanoparticle-formed nanofluids: Molecular dynamics simulation investigation of argon-based nanofluids

https://doi.org/10.1515/ntrev-2024-0058
received February 8, 2024; accepted June 20, 2024

Abstract: The influence of nanoparticle shape, volume fraction, and temperature on the thermal properties of nanofluids plays a pivotal role in engineering applications. However, there remains a considerable lack of systematic research comprehensively considering these factors to study the similarities and differences in the thermal properties of nanofluids composed of metals and their oxides and to conduct in-depth analyses of their internal mechanisms and characteristics. In this study, molecular dynamics simulations were conducted, employing reversing perturbation non-equilibrium molecular dynamics and non-equilibrium molecular dynamics methods. The thermal conductivity and viscosity of Al–Ar and Al_2O_3–Ar nanofluids were thoroughly investigated under the various influencing factors. Results reveal that under identical conditions, the thermal conductivity of Al–Ar nanofluid surpasses that of Al_2O_3–Ar nanofluid, exemplified by values such as 0.1832 W/m K (Al–Ar, 1.5%, cylinder, 86 K) *versus* 0.17745 W/m K (Al_2O_3–Ar, 1.5%, cylinder, 86 K). Furthermore, the viscosity of Al–Ar nanofluid is lower than that of Al_2O_3–Ar nanofluid, demonstrated by values such as 0.0004882 Pa S (Al–Ar nanofluid, 86 K, 2.5%, platelets) compared to 0.008975 Pa S (Al_2O_3–Ar nanofluid, 86 K, 2.5%, platelets). Subsequently, this study analyzed the difference in thermal conductivity between the two nanofluids from the perspective of microscale interface heat conduction by comparing the phonon density of states curves of Al, Ar, and Al_2O_3 in the two nanofluids for overlap. Subsequently, through radial distribution function analysis, the viscosity difference between Al–Ar and Al_2O_3–Ar nanofluids is explained based on nanofluid–solid interface and microstructural considerations. This research addresses the comprehensive lack of comparative studies on the thermal properties of nanofluids formed by metals and their oxides. The internal mechanisms underlying the thermal property differences of nanofluids formed by metals and their oxides were revealed from a microscopic perspective, which holds significant implications for the engineering applications of nanofluids.

Keywords: nanofluid, metals and their oxides, molecular dynamics simulation, phonon density of states, radial distribution function

1 Introduction

Nanofluids are functional fluids formulated by dispersing metal, metal oxide, or other non-metal nanoparticles (NPs) with exceptional suspension capabilities into a base fluid (BF), thereby achieving superior thermophysical properties. Due to their outstanding thermal characteristics, nanofluids have recently received widespread attention in fields requiring high heat transfer efficiency, such as microelectronics cooling, air conditioning, mechanical friction, and other related applications [1–5].

As mentioned earlier, nanofluids exhibit exceptional thermophysical properties, among which the most notable are their high thermal conductivity [6–9] and acceptable viscosity characteristics compared to heat transfer fluids formed with micrometer-sized particles in BFs. These

* **Corresponding author: Zhumei Luo**, Faculty of Metallurgical and Energy Engineering, Kunming University of Science and Technology, Kunming, 650093, China, e-mail: 13662033682@163.com
* **Corresponding author: Shan Qing**, Faculty of Metallurgical and Energy Engineering, Kunming University of Science and Technology, Kunming, 650093, China, e-mail: steam1ch@126.com
Chenghang Li, **Haoming Huang**, **Xiaohui Zhang:** Faculty of Metallurgical and Energy Engineering, Kunming University of Science and Technology, Kunming, 650093, China

thermophysical properties have been well studied in recent years. Nanofluids, characterized by high thermal conductivity [6–9] and acceptable viscosity compared to heat transfer fluids formed with microparticles in the base liquid, have been extensively investigated for their outstanding thermal properties. Minakov *et al.* [10] explored the thermal conductivity of water-based Al_2O_3 nanofluids at various volume concentrations (1–6%). Results showed an increase in thermal conductivity by up to 1.24 times.

Kanti *et al.* [11] investigated the effect of pH value on the stability and thermal performance of hybrid nanofluids (HNFs) consisting of copper oxide (CuO) and graphene oxide (GO) at different mixing ratios. This study provides significant guidance for understanding the influence of pH value on the thermal properties and stability of nanofluids. The researchers [12] employed molecular dynamics to investigate the boiling flow characteristics of copper–water nanofluids in nanochannels with varying roughness. Additionally, they examined the influence of the Lennard–Jones (L–J) potential function on gas–liquid-phase equilibrium and conducted molecular dynamics simulations of annular flow boiling. Kanti *et al.* [13] investigated the specific heat, dynamic viscosity, and thermal conductivity of water-based Indian coal fly ash-stable nanofluid containing 0.1–0.5% volume concentration of Indian coal fly ash NPs over the temperature range of 30–60°C. The study found that the thermal conductivity and viscosity of the fly ash nanofluid increased with increasing volume fraction, while the specific heat capacity decreased with increasing volume fraction. Both thermal conductivity and specific heat were directly proportional to temperature, whereas viscosity was inversely proportional.

Agarwal *et al.* [14] employed the transient line heat source method to investigate Al_2O_3 nanofluids, finding a 13% increase in thermal conductivity at temperatures below 10°C and varying volume fractions (ranging from 0 to 2%). Shinde *et al.* [15] studied the thermal conductivity of water-based Al_2O_3 nanofluids, observing an increase with the rise in NP volume concentration. Kanti *et al.* [16] investigated the dispersion stability and thermal properties of water-based alumina (Al_2O_3), GO, and their HNFs at various mixing ratios. They also established a model using machine learning techniques to accurately predict the thermal conductivity and viscosity of the water-based alumina (Al_2O_3) and GO HNFs. Topal and Servantie [17] discovered that as the volume fraction increased, the enhancement in thermal conductivity of water-based Al_2O_3 nanofluids gradually diminished. Hamid *et al.* [18] studied the thermophysical properties of TiO_2-SiO_2 nanofluids with water and ethanol in different ratios. The results showed that the optimal mixing ratios for TiO_2-SiO_2 nanofluids are 40:60 and 80:20, with greater improvements in thermal conductivity and dynamic viscosity compared to other mixing.

In recent years, extensive research has been conducted on the factors influencing the exceptional thermophysical properties of nanofluids. These factors primarily include the aggregation of NPs within the nanofluids, the shape of NPs, the volume fraction of the nanofluid, and temperature conditions.

In recent years, numerous studies have demonstrated that one of the key factors contributing to the enhanced thermal conductivity of nanofluids is the aggregation of NPs within the nanofluids [17,19–24]. Extensive research has been conducted on this phenomenon. Guo and Zhao [25] investigated the thermal conductivity of Cu–Ar nanofluid systems using the equilibrium molecular dynamics method in molecular dynamics and explored the impact of fractal dimension on the thermal conductivity of Cu–Ar nanofluid systems. The findings indicate that with constant NP volume fraction and size, the smaller the fractal dimension of the nanofluid, the greater its thermal conductivity. Zhou *et al.* [26] studied the influence of NP aggregation on the thermal conductivity and viscosity of oil-based nanofluids with metal NPs. Experimental studies on nanofluids formed by magnetic iron oxide NPs [27] have shown that the thermal conductivity significantly increases when the NPs form chain-like aggregates within the nanofluid.

Feng *et al.* [28] investigated the relationship between NP size and thermal conductivity in nanofluids through an NP aggregation model, demonstrating that thermal conductivity increases as the size of NPs decreases. Hong and Kim [22] and others, using molecular dynamics simulations, found that the aggregation of NPs enhances the thermal conductivity of nanofluids. For instance, Thajudeen and Hogan [29] explored the thermal conductivity of nanofluids under different aggregation structures, finding that, with a constant volume fraction, the thermal conductivity of nanofluids could increase by 51% or decrease by 32% depending on the aggregation structure.

However, the details of heat transfer in nanofluids remain incompletely understood, and research on the mechanisms controlling the enhanced thermal conductivity of nanofluids is limited. Therefore, it is necessary to further investigate the underlying mechanisms of how the internal properties of NPs, as well as various factors such as volume fraction, shape, and temperature, affect thermal conductivity, viscosity, and other thermal properties in specific nanofluids.

In the study of the thermal–physical properties of nanofluids, the influence of NP shape factors on properties such as thermal conductivity and viscosity has gradually garnered widespread attention. In the study investigating

the relationship between NP shape and the thermal–physical properties of nanofluids, the surface area-to-volume ratio (*S*/*V* ratio) of NPs has increasingly attracted researchers' attention. It primarily refers to the ratio of the surface area value of NPs to the volume value of NPs, and in relevant studies, its value is closely associated with the thermal conductivity of nanofluids.

Main *et al.* [30] studied Al_2O_3-1-butyl-3-methylimidazolium bis(trifluoromethylsulfonyl) imide ((C4 mim) (NTf2)) nanofluids and found that the thermal conductivity varies with different NP shapes, with needle-shaped NPs forming nanofluids exhibiting the highest thermal conductivity due to their higher *S*/*V* ratio. Zhang *et al.* [31] conducted a detailed study on the influence of NP shape (*S*/*V* ratio) on the thermal conductivity of Cu–Ar nanofluids. The results indicate that the thermal conductivity of nanofluids increases with the increase in the *S*/*V* ratio of NPs.

Zhu *et al.* [32] explored the thermal conductivity of CuO-dimethicone nanofluids with different shapes of NPs, revealing that nanofluids composed of spherical NPs had lower thermal conductivity compared to those formed by linear NPs. Furthermore, the thermal conductivity increased with an elevation in NP concentration. Kanti *et al.* [33] investigated the effect of NP size on the thermal conductivity and dynamic viscosity of stable water-based Indian coal fly ash nanofluid. The study revealed that the stability, thermal conductivity, and dynamic viscosity of stable water-based Indian coal fly ash nanofluid increased with decreasing particle size, while viscosity decreased with increasing temperature.

Maheshwary *et al.* [34] conducted a study on water-based nanofluids comprising NPs of different shapes such as Al_2O_3, CuO, TiO_2, MgO, and ZrO_2. The study results demonstrated that the nanofluid with a volume fraction of 2.5% of "U"-shaped Al_2O_3 exhibited the highest viscosity. Studies by Wang *et al.* [35] and Jin *et al.* [36] indicate a significant impact of NP size on nanofluid viscosity, with changes in NP size resulting in a 12.8% decrease in viscosity.

Based on the comprehensive analysis of the current research status on nanofluids, it is evident that the current focus in the study of the thermal properties of nanofluids primarily centers around the influence of factors such as thermal conductivity, viscosity, and various other aspects.

However, there are a limited number of studies that provide a comprehensive comparison of nanofluids composed of a particular metal and its corresponding metal oxide in terms of thermal conductivity, viscosity, stability, etc. Moreover, there is a notable lack of research that thoroughly considers the impact of factors, such as NP shape, volume fraction, and *S*/*V* ratio, on the differences in thermal conductivity, viscosity, stability, and other aspects of nanofluids composed of a metal and its corresponding metal oxide.

Additionally, there is a significant gap in studies that provide explanations for these differences from the perspective of phonon heat transport. This has resulted in our understanding of the thermal properties of nanofluids composed of each metal and its corresponding metal oxide individually, but it remains unclear why their thermal properties differ. The internal mechanisms underlying these differences have not been thoroughly investigated from a microscopic perspective, and universal conclusions have not been drawn. A deeper exploration of the microscopic mechanisms could allow us to extend our conclusions to all nanofluids composed of metals and their oxides in the same type of BF, elucidating their similarities and differences in thermal properties. Such insights would hold significant theoretical and practical implications for the engineering applications of nanofluids.

In this study, comprehensive molecular dynamics simulations and analyses were performed on the nanofluidic systems under investigation using the LAMMPS program. The non-equilibrium molecular dynamics (NEMD) method, along with the reversing perturbation non-equilibrium molecular dynamics (RNEMD) method, was employed to conduct detailed computational and analytical investigations. The primary objective of this article is to comprehensively analyze the differences in thermal conductivity, viscosity, and microscopic structures of nanofluids formed by metallic NPs and their corresponding metal oxides. Various factors, such as NP shape, *S*/*V* ratio, temperature, and volume fraction, were systematically varied to elucidate the comprehensive mechanism underlying the differences. A phononic perspective was employed to analyze these distinctions. Furthermore, methods such as phonon density of states (PDOS) and radial distribution functions (RDFs) have been utilized to analyze these differences from a microscopic perspective. To gain insights into the microscopic mechanisms and structural characteristics of nanofluids composed of metals and their oxides, molecular dynamics simulation methods were further applied. The RDFs with different shapes, temperatures, and volume fractions of metallic and metal oxide NPs were thoroughly computed and analyzed.

Given the representative nature of Al and Al_2O_3 in constructing nanofluids, owing to their excellent thermodynamic properties, they are among the most common heat transfer fluids. Therefore, Al and Al_2O_3 were selected as the metallic NPs in this study. Argon (Ar) was chosen as the BF for the nanofluid. The reason for choosing Ar-based nanofluids as the subject for our study is twofold: first, Ar-based nanofluids are an ideal choice for investigating the thermal–physical properties of various nanofluids using molecular dynamics. Kang and colleagues described the interatomic potential between Ar atoms using the well-

known L–J potential and employed the more accurate embedded atom method potential to describe the interatomic interactions between NP atoms. Therefore, the potential energy parameters for Ar align very closely with experimental data, making Ar-based nanofluids a suitable subject for research. This choice facilitates the extension of theoretical models to experiments [23,31,37–43] and ensures a certain level of representativeness.

The second reason is that the computational burden is significantly reduced when using the two-body L–J potential compared to multi-body potential. Furthermore, the accuracy of thermal flow calculations using the two-body potential exceeds that of multi-body potential [31,38,41,43].

2 Simulation methodology

2.1 Potential energy function and parameters

In this study, nanofluidic systems were established with Ar liquid as the BF and Al, as well as Al_2O_3, as the NPs. Molecular dynamics simulations were carried out using the LAMMPS package, and computational results were observed and atomically visualized using Ovito [44].

In terms of model construction, the interatomic potentials between all Ar atoms and between Al atoms and Ar atoms in the Al–Ar nanofluid were described by the pairwise 12–6 L–J potential. This potential can be directly applied to calculate the interatomic interactions between Al–Ar and Ar–Ar in the nanofluidic system, with the computational formula as follows [45]:

$$\varphi(r_{ij}) = 4\varepsilon\left[\left(\frac{\sigma}{r_{ij}}\right)^{12} - \left(\frac{\sigma}{r_{ij}}\right)^{6}\right] (r < r_c). \tag{1}$$

The mixed interatomic potential parameters between Al and Ar atoms in the Al–Ar nanofluidic system were calculated using the Lorentz–Berthelot rule, with the computational formula as follows:

$$\varepsilon_{\mathrm{Al-Ar}} = \sqrt{\varepsilon_{\mathrm{Al}} \times \varepsilon_{\mathrm{Ar}}}, \tag{2}$$

$$\sigma_{\mathrm{Al-Ar}} = \left[\frac{\sigma_{\mathrm{Al}} + \sigma_{\mathrm{Ar}}}{2}\right], \tag{3}$$

where ε represents the energy constant; σ represents the length constant; r_{ij} represents the distance between atoms i and j; and r_c represents the cutoff radius, typically where $r_c > 2.5\sigma$, and in this study, $r_c = 11$ Å. The specific L–J potential parameters are presented in Table 1.

Table 1: L–J potential parameters used in this study

Atom	ε/eV	σ/Å
Ar–Ar	0.01051	3.405
Al–Al	0.39217	3.012
Al–Ar	0.0462	3.0125

Modeling of the Al_2O_3–Ar nanofluidic system was conducted using Materials Studio. The crystalline structure of Al_2O_3 and the atomic model of Ar were established. Subsequently, the Al_2O_3 structure was introduced into a box filled with Ar atoms. The COMPASS II and consistent valence force fields were employed, and the output was formatted into an LAMMPS-recognizable data model file. Harmonic potentials were used in this model to describe bond angles and dihedral parameters. The generated model files were then coupled with the LAMMPS program for molecular dynamics simulation.

2.2 Thermal conductivity calculation protocol

The most notable advantageous thermal property of nanofluids is their higher thermal conductivity compared to the pure BF, making them ideal heat transfer fluids. Therefore, this study aims to investigate the thermal conductivity of Al–Ar nanofluids and Al_2O_3–Ar nanofluids, exploring their correlations and differences.

The NEMD method was employed in this study to calculate the thermal conductivity of nanofluids [17]. In applying this method, it is essential to define the direction of heat flow. In this study, the heat flow was specified to occur along the X-axis, and macroscopically, the heat transfer phenomenon follows Fourier's law. Subsequently, temperature ranges were set within the simulation system to generate an appropriate temperature difference, thereby inducing a temperature gradient over a certain period and allowing the system to reach a steady state. Finally, temperature data were computed by LAMMPS to determine the temperature gradient. The thermal conductivity was then calculated using the formula [46]:

$$K = -\frac{J}{A \times \nabla T}, \tag{4}$$

$$\nabla T = \frac{\partial T}{\partial x}, \tag{5}$$

$$J = \frac{\Delta \varsigma}{2\Delta t}. \tag{6}$$

In Eq. (4), K represents thermal conductivity, J denotes the heat flux density in the system, A is the cross-sectional area perpendicular to the direction of heat flow, and ∇T is the temperature gradient along the X-axis.

In Eq. (5), X represents the direction of heat transfer. During the simulation process, this aspect employed the NEMD method proposed by Hafskjold and Ikeshoji. To induce a temperature variation in the system and establish a temperature gradient, the "fix ehex" command was applied to set the heat flux density J.

In Eq. (6), $\Delta ç$ represents the heat transferred in the system, t signifies the designated time step. The factor of 2 in the denominator accounts for the periodic boundary conditions set for the system. To avoid redundant calculations in both directions of heat flow, the entire formula is divided by 2.

Figure 1 illustrates the detailed information about the system's heat flux, heat, and the subdivision rule. During molecular dynamics simulation, the research divided the simulation box into 20 blocks, with atoms uniformly distributed within each designated region. Subsequently, a heat source area and a cold sink area were defined. The "fix ehex" command was employed to input and extract heat in the heat source and cold sink areas, thus creating a heat source and sink. This process generated temperature variations in the simulation system, establishing a temperature gradient. The details of this process are depicted in Figure 1.

2.3 Viscosity calculation protocol

In the research on the thermal properties of nanofluids using molecular dynamics, the study of viscosity is essential [31,43].

In this study, we utilized the shear viscosity calculation method based on (RNEMD), also known as the Müller-Plathe method [47]. Figure 2 illustrates the schematic diagram of this method. The system is initially divided into 20 bins along the Z-axis, and the atomic velocity component V_x in the X-direction is established. The velocity gradient of V_x is created by exchanging momentum components P_x of atoms in the X-direction between the first bin, the 20th bin, and the 11th bin. This process forms a shear field and generates a momentum flux $J_z(P_x)$ across the plane A (the plane formed by the X- and Y-axes). The momentum exchange values in the Z-direction are then recorded during the momentum exchange process and used for viscosity calculation [48]. The calculation formula is as follows:

$$J_Z(P_x) = -\eta \frac{\partial v_x}{\partial Z}, \tag{7}$$

$$\eta = -\frac{\sum(P_{x,1} - P_{x,11})}{2\Delta t L_x L_Y [\partial v_x/(\partial Z)]}. \tag{8}$$

In Eq. (7), η represents the shear viscosity, where $\frac{\partial v_x}{\partial Z}$ is the velocity gradient of V_x in the Z-direction. After a series of transformations, Eq. (7) is converted to Eq. (8). Eq. (8) is the primary formula used in LAMMPS simulation calculations

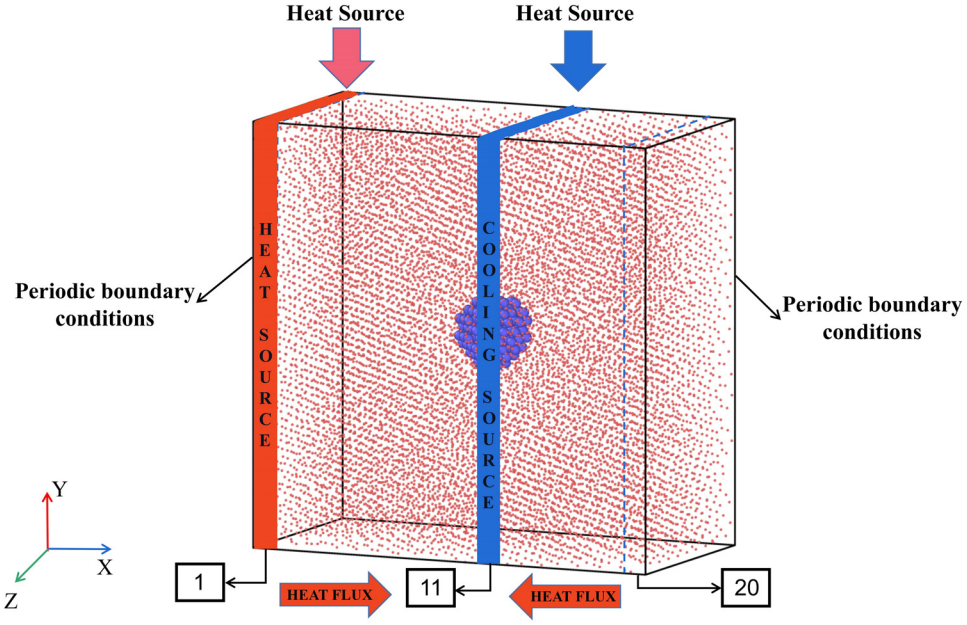

Figure 1: Schematic diagram of the subdivision setting and distribution of the heat source and cold sink along the X-axis in the nanofluid simulation system.

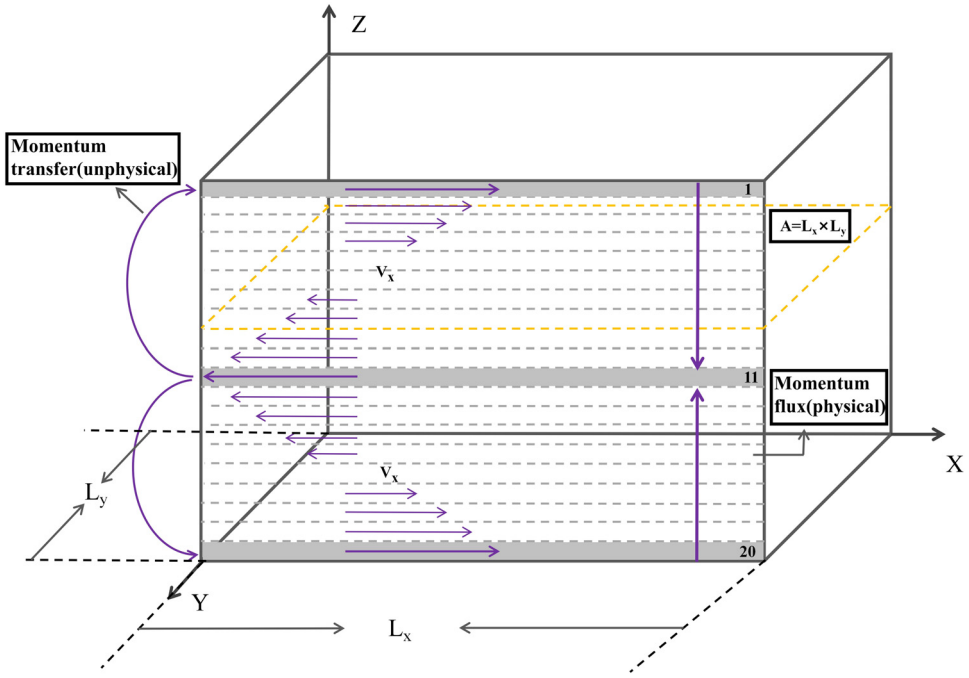

Figure 2: Schematic diagram illustrating the principle of shear viscosity calculation using the MP method.

for shear viscosity, where $P_{x,1}$ and $P_{x,11}$ correspond to the momentum values in the first bin and the 11th bin.

2.4 Calculation of RDF

To gain a deeper understanding of the obtained thermal conductivity and viscosity patterns of nanofluids, this study calculated the RDF of the two nanofluids to explore their microscopic mechanisms from the perspective of atomic interactions [49]. In the RDF, $g(r)$ represents the probability of neighboring atoms occurring around a central atom at a specified distance. The calculation formula is as follows [50]:

$$(r) = \frac{V}{n_a n_b} \sum_{i=1}^{n_a} \frac{n_{ib}(r, \Delta r)}{4\pi r^2 \Delta r}, \tag{9}$$

where V represents the volume of the simulated system, n_a and n_b denote the quantities of particles a and b, and $n_{ib}(r, \Delta r)$ represents the number of particles b within the distance range from r to Δr.

2.5 Establishment of simulation model

To comprehensively investigate the correlations and differences in thermal properties such as thermal conductivity and viscosity between metals and their oxides, this study conducted molecular dynamics simulations. Prior to the simulations, the models were established with the following details. Initially, simulation boxes were created with dimensions of 100 Å in the *X*-direction, 50 Å in the *Y*-direction, and 100 Å in the *Z*-direction. These boxes were filled with Ar atoms, and different shapes (cylinder, sphere, cube, platelets) and quantities (controlling the volume fraction of the nanofluid system at 0.5, 1, 1.5, 2, and 2.5%) of Al NPs and Al_2O_3 NPs were subsequently introduced into the Ar-filled systems. This process resulted in the formation of Al–Ar nanofluids and Al_2O_3–Ar nanofluids with varying NP shapes and volume fractions. The details of NP shapes and sizes are illustrated in Figure 3 and Table 2. The rules for heat transfer and subdivision are described in Section 2.2 and detailed in Figure 1.

2.6 Simulation model verification

To validate the correctness of the established simulation model, this study conducted simulation calculations. Initially, thermal conductivity simulations were performed on the Al–Ar nanofluid system at 85 K. The thermal conductivity calculations in this study followed the following procedure: 1) “fix ehex” command was used to apply input and output heat flows to create heat sources and sinks in the system. 2) The system simulation box was divided into 20 layers along the *X*-axis, each with a thickness of 5 Å. The heat source was set in the 1st layer, and the cold sink was set in the 11th layer. The entire system’s

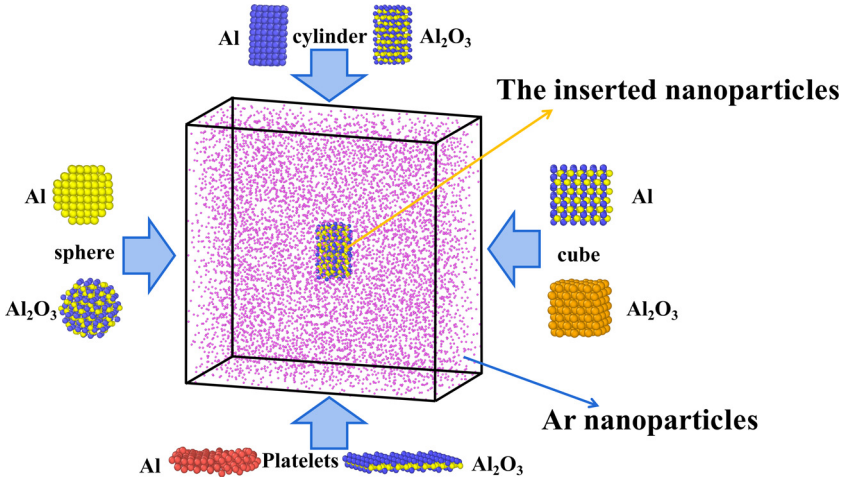

Figure 3: Schematic diagram depicting the details of NP shapes and simulation box dimensions.

boundary conditions were set as periodic boundary conditions, enabling uniform heat transfer along the *X*-axis. For the thermal conductivity calculations of the Al–Ar nanofluid system at 86 K and a volume fraction of 1%, the procedure was as follows: first, the temperature was set to 86 K. Then, the "fix ehex" command was used to set the input and output energy to 0.05 ev/ps (following the metal unit system in LAMMPS). Subsequently, under the conditions of a time step of 2 fs, 300,000 relaxation steps (0.6 ns) were performed in the canonical ensemble (NVT) to stabilize the temperature at 86 K. Then, the NEMD method was applied in the microcanonical ensemble (NVE) for thermal conductivity calculations.

During the calculation process, the temperature variation across the 20 layers was monitored. The monitoring results, shown by the orange curve in Figure 4, indicate that when the simulation steps reached 300,000, the temperature gradient represented by the orange temperature curve approached a V-shaped segment. This indicates that the simulation system we established is scientifically sound and has achieved excellent NEMD simulation. Ultimately, the obtained thermal conductivity was 0.1828 W/m K. Comparing this with the value of 0.183 W/m K calculated in the study by Li *et al.* [51], the error is 0.00109%. This negligible difference demonstrates the stability and reliability of our simulation system. This comparative result is presented in Figure 5.

After validating the thermal conductivity calculation method, we proceeded to verify the rationality of the viscosity calculation method. First, following the scheme illustrated in Figure 2, the simulation system was divided into 20 bins along the *Z*-axis. By exchanging the momentum components P_x of atoms in the *X*-direction between the first bin, the 20th bin, and the 11th bin, a velocity gradient for V_x was established, forming a shear field. The viscosity was eventually calculated as outlined in Section 2.4 and depicted in Figure 2. In this part of the study, due to limited viscosity data available for reference in the case of Al–Ar, we chose to validate the viscosity calculation method using the Cu–Ar nanofluid system at 90 K and a volume fraction of 1.29%. Initially, after multiple linear calculations of velocity gradients with a momentum exchange frequency of

Table 2: Details of NP size parameters

NPs	Cylinder	Sphere	Cube	Platelets
S/V value	0.31746	0.357	0.441176	0.805
Dimension	$20Å \times 6.3Å$	$8.4Å$	$3.6Å$	$28.9Å \times 3Å$
	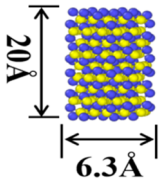	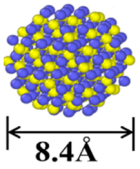	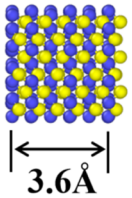	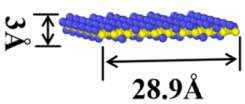

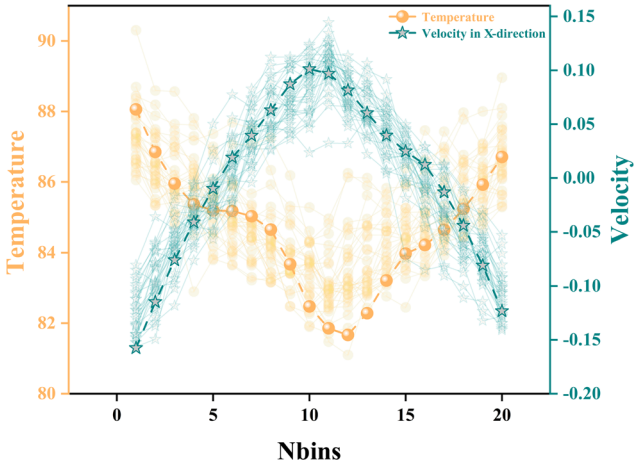

Figure 4: Temperature and velocity gradient within the 20 layers of the simulation system.

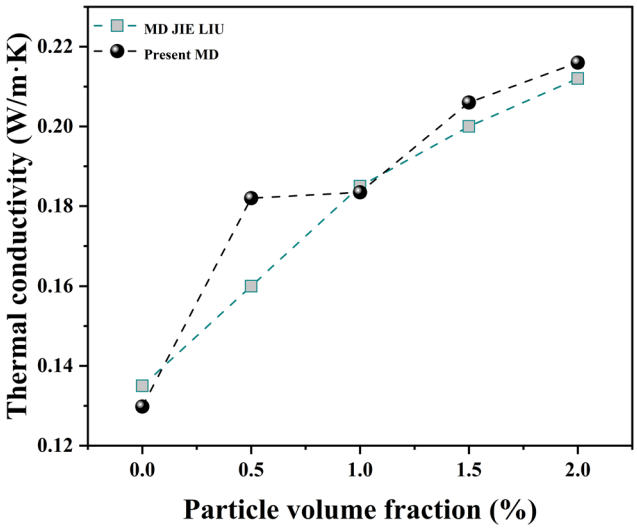

Figure 5: Comparison of thermal conductivity of Al–Ar nanofluid with existing research results [51].

N = 5, the NPT ensemble was employed to run 300,000 steps, maintaining the temperature at 90 K with a time step of 2 fs. Subsequently, 300,000 steps were run in the NVT, monitoring the system's velocity distribution along the X-axis to obtain the velocity distribution curve (depicted as the green curve in Figure 4). The observed V-shaped velocity curve indicates that a stable and rational velocity gradient was achieved in the X-direction. The calculated viscosity value for the Cu–Ar nanofluid system at 90 K and a volume fraction of 1.29% was 2.91×10^{-4} Pa S. Comparing this with the existing research value of 2.92×10^{-4} Pa S [43], the error is 0.00342%, demonstrating the stability and reliability of our simulation system. This comparative result is illustrated in Figure 6.

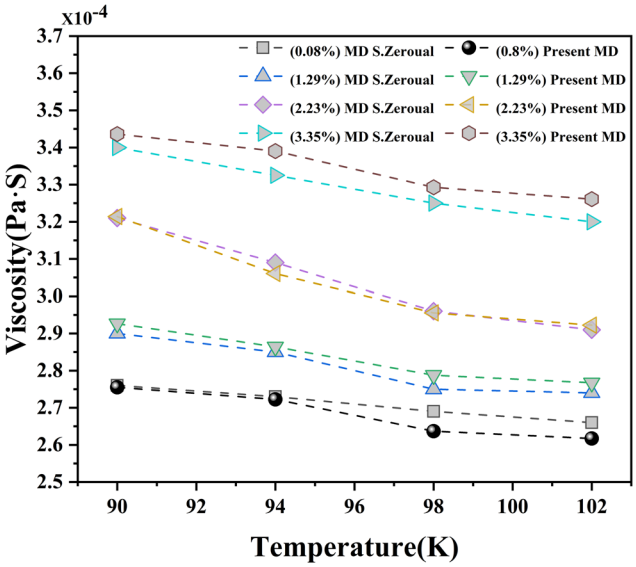

Figure 6: Comparison of viscosity of Cu–Ar nanofluid with existing research results [43].

We further conducted a series of model and code correctness validations. Initially, we validated the thermal conductivity of Al–Ar nanofluid at different volume fractions at 86 K, as shown in Figure 5. The results indicated a high similarity between our calculated values and existing research, with an overall trend of increasing thermal conductivity with higher volume fractions of Al–Ar nanofluid. Subsequently, we validated the viscosity of Cu–Ar nanofluid under different temperatures and volume fractions, as depicted in Figure 6. The results demonstrated a close resemblance between our study's outcomes and existing calculations, with a general trend of decreasing viscosity as the temperature increased and increasing viscosity with higher volume fractions. Finally, we validated the thermal conductivity of Cu–Ar nanofluid at various volume fractions, as presented in Figure 7. The results indicated a high similarity between our calculated values and existing research, with an overall trend of increasing thermal conductivity at higher volume fractions. This series of validations concludes that the simulation system established in this study is stable, reliable, and trustworthy.

3 Simulation results and analysis

3.1 Effect of NP shape and temperature on the thermal conductivity and viscosity of Al–Ar nanofluid

This section investigates the influence of four different NP shapes (cylinder, sphere, cube, and platelets) along with

different temperatures on the thermal conductivity and viscosity of Al–Ar nanofluid.

We present the research findings on the influence of NP shape and different temperatures on the thermal conductivity of Al–Ar nanofluid in the form of bar graphs in Figure 8. From Figure 8(a–e), it is visually evident that the thermal conductivity of Al–Ar nanofluid increases with rising temperatures. Moreover, nanofluids formed by NPs with higher shape factors (S/V values) exhibit higher thermal conductivity. Specifically, the nanofluid with plate-like NPs (a maximum S/V value of 0.805) achieves the highest thermal conductivity at each volume fraction. The corresponding values are 0.162 W/m K (0.5%, 106 K, platelets), 0.198 W/m K (1%, 106 K, platelets), 0.20997 W/m K (1.5%, 106 K, platelets), 0.237 W/m K (2%, 106 K, platelets), and 0.248 W/m K (2.5%, 106 K, platelets). Previous studies suggest that the increase in nanofluid thermal conductivity is primarily due to the random motion of NPs within the nanofluid, known as Brownian motion [52]. According to this theory, an increase in the intensity of Brownian motion of NPs in the nanofluid leads to more nanofluid base liquid molecules flowing from the high-temperature region to the low-temperature region. This, in turn, enhances the temperature transfer efficiency within the nanofluid, resulting in higher thermal conductivity [33]. Koo and Kleinstreuer's research indicates that the Brownian motion of NPs in nanofluid significantly intensifies as the temperature rises. Therefore, nanofluid thermal conductivity increases with the elevated environmental temperature [53]. Thus, our study's results also indicate that the increase in nanofluid thermal conductivity with rising environmental temperature is attributed to the more intense Brownian motion of NPs at higher temperatures, leading to a higher nanofluid thermal conductivity.

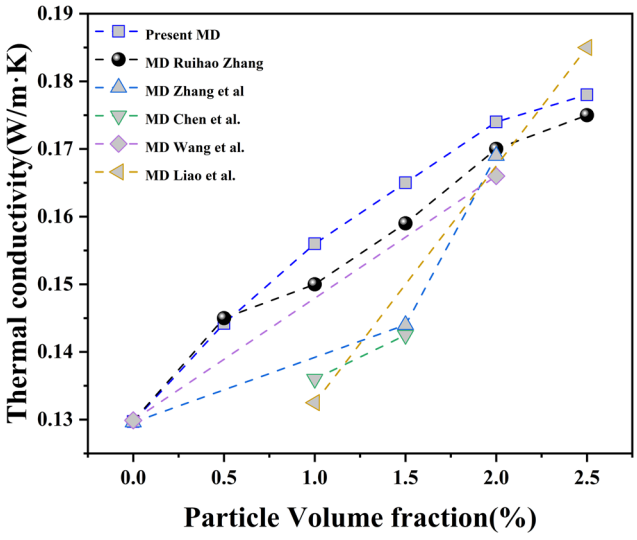

Figure 7: Comparison of thermal conductivity of Cu–Ar nanofluid with existing research results [31].

In order to delve deeper into the influence of NP shape (S/V ratio) on the thermal conductivity of nanofluids, this study further investigates the relationship between the growth rate of thermal conductivity and the S/V ratio. Liao *et al.* [41] have determined the thermal conductivity of pure Ar fluid to be 0.129 W/m K. This study calculates the growth rate of thermal conductivity relative to pure Ar fluid for Al–Ar nanofluid at a volume fraction of 0.5% and a temperature of 106 K. The growth rate of thermal conductivity is as follows: 9.15% (cylinder, S/V = 0.31746), 12.4% (sphere, S/V = 0.357), 16.4% (cube, S/V = 0.441176), and 25.6% (platelets, S/V = 0.805). We visually present the results in Figure 8(f). From Figure 8(f), it can be observed that under the same simulation conditions, as the S/V ratio of NPs increases (indicated by the black portion in the figure), the growth rate of thermal conductivity of nanofluids gradually increases (indicated by the green portion in the figure). Previous studies suggest that the main reason for the variation in thermal conductivity with the S/V ratio is due to the surface effects of NPs [54]. Maheshwary *et al.* [55], in their study on the thermal conductivity of TiO_2–H_2O nanofluids, emphasized the crucial role of the surface area of TiO_2 NPs in influencing the thermal conductivity of TiO_2–H_2O nanofluids. Therefore, NPs with different shapes and hence different surface areas have a significant impact on the thermal conductivity of nanofluids. Cui *et al.* [56], in their research on the thermal conductivity of NPs, indicated that the ratio of energy atoms in NPs (E) is a standard for assessing the influence of NPs on nanofluid thermal conductivity. As E increases with the increase in the S/V ratio of NPs, the growth rate of thermal conductivity in this study increases with the larger S/V ratio of NPs.

We present the research results on the influence of NP shape and different temperatures on the viscosity of Al–Ar nanofluids in the form of bar charts in Figure 9. From Figure 9(a–e), it can be visually observed that the viscosity of Al–Ar nanofluids decreases with increasing temperature. Moreover, the viscosity of Al–Ar nanofluids is minimally affected by changes in NP shape, exhibiting only slight fluctuations without significant variation. From the figure, we observe a gradual decrease in viscosity with increasing temperature. For each volume fraction, the highest and lowest viscosity values are as follows: for an NP volume fraction of 0.5%: highest value: 0.0003096 Pa S (0.5%, 86 K, cube), lowest value: 0.0002045 Pa S (0.5%, 106 K, platelets). For an NP volume fraction of 1%: highest value: 0.0003592 Pa S (1%, 86 K, cube), lowest value: 0.000242 Pa S (1%, 106 K, platelets). For an NP volume fraction of 1.5%: highest value: 0.0003893 Pa S (1.5%, 86 K, sphere), lowest

value: 0.00027 Pa S (1.5%, 86 K, platelets). For an NP volume fraction of 2%: highest value: 0.000435887 Pa S (2%, 86 K, platelets), lowest value: 0.0002731 Pa S(2%, 106 K, platelets). For an NP volume fraction of 2.5%: highest value: 0.0004882 Pa S (2.5%, 86 K, platelets), lowest value: 0.000325 Pa S (2.5%, 106 K, cube).

The phenomenon of decreasing viscosity with increasing temperature aligns with numerous existing study results [57].

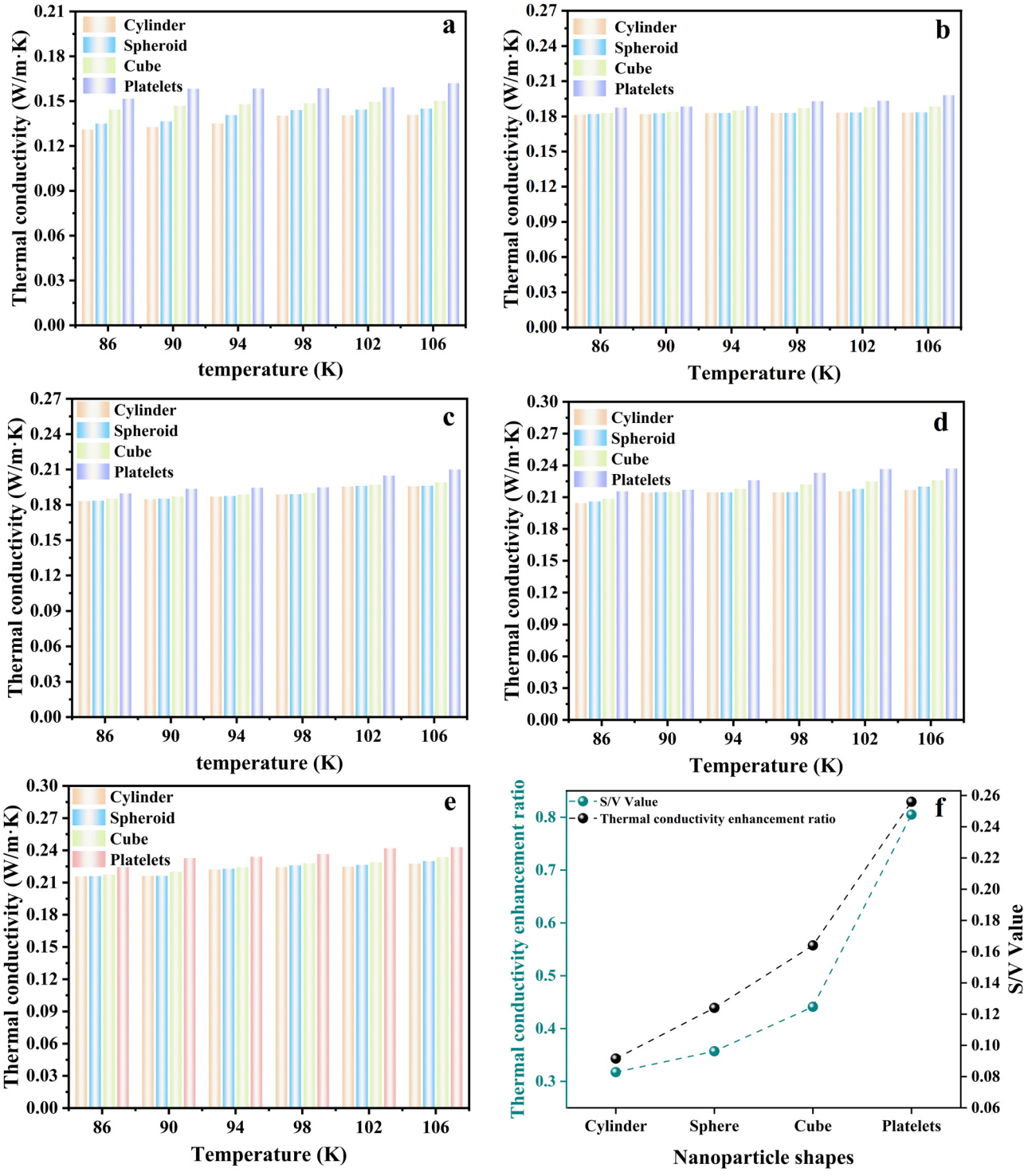

Figure 8: Variation patterns of thermal conductivity of Al–Ar nanofluids with temperature and shape factor (*S*/*V* ratio). (a) 0.5%, (b) 1%, (c) 1.5%, (d) 2%, (e) 2.5%.

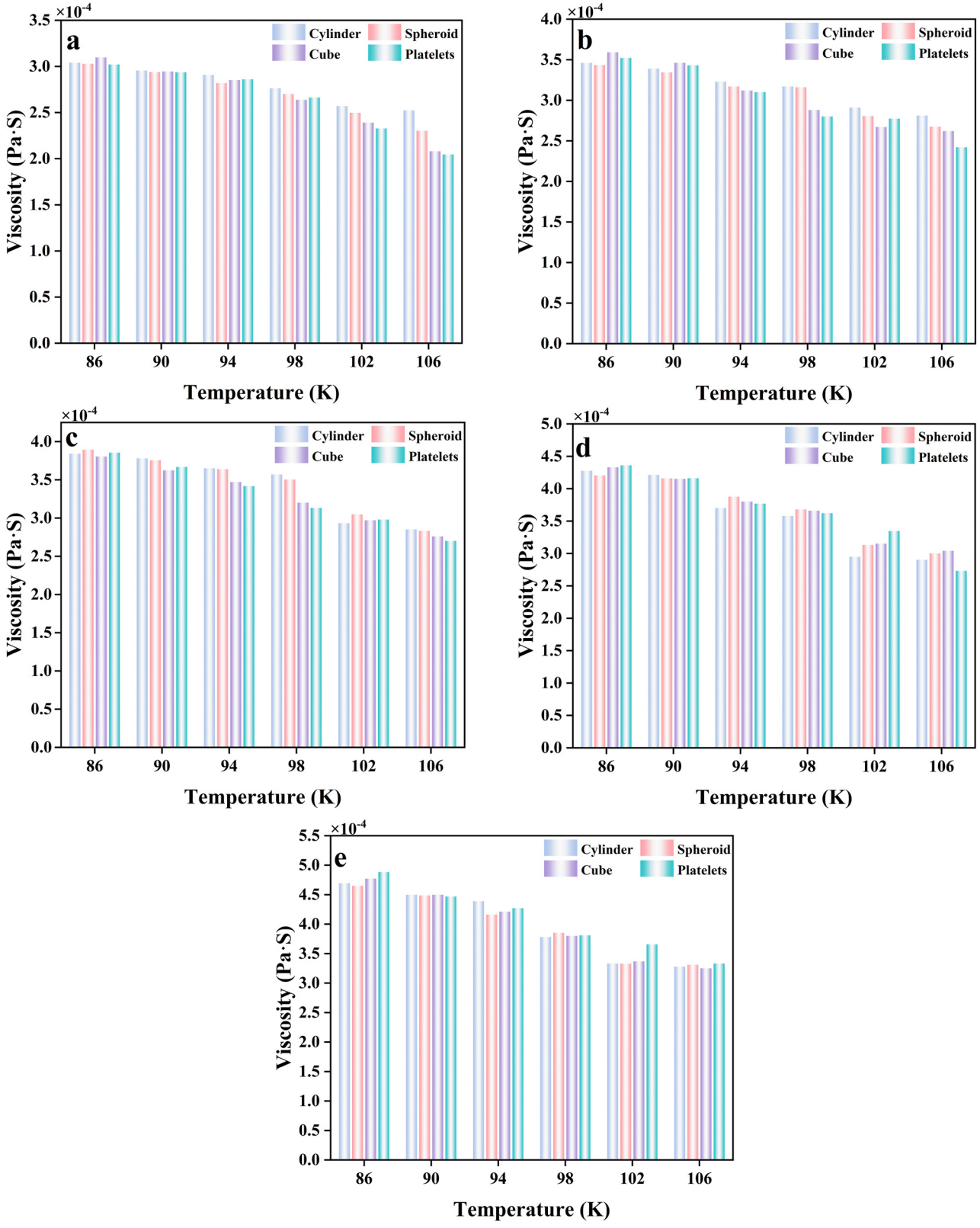

Figure 9: Variation patterns of viscosity of Al–Ar nanofluids with temperature and shape factor (*S*/*V* ratio). (a) 0.5%, (b) 1%, (c) 1.5%, (d) 2%, (e) 2.5%.

Prior studies have investigated the patterns of viscosity variation with temperature and established theoretical models. For instance, Masoumi *et al.* [58] developed a theoretical model based on the Brownian motion of NPs in nanofluids, predicting nanofluid viscosity under conditions such as average particle diameter, NP density, BF properties, and environmental temperature. The predicted results from this model align with the findings of our study, indicating a decrease in nanofluid viscosity with increasing temperature. Ranjbarzadeh *et al.* [59] demonstrated that, in fluids, molecules can overcome adhesive forces within the fluid with increasing thermal energy, leading to a decrease in fluid viscosity with rising temperature. Additionally, temperature increase results in an expansion of gaps between the BF and NPs in nanofluids, reducing the resistance to nanofluid flow and consequently lowering viscosity.

3.2 Effect of NP volume fraction on the thermal conductivity and viscosity of Al–Ar nanofluids

In this section, we investigate the impact of different NP shapes and volume fractions on the thermal conductivity and viscosity of Al–Ar nanofluids. Similar to the previous section, the NP shapes considered are cylinder, sphere, cube, and platelets.

The study results on the influence of different volume fractions of NPs on the thermal conductivity of Al–Ar nanofluids are presented in Figure 10. From Figure 10(a–d), the variations in Al–Ar nanofluid thermal conductivity with volume fraction and temperature are visually depicted.

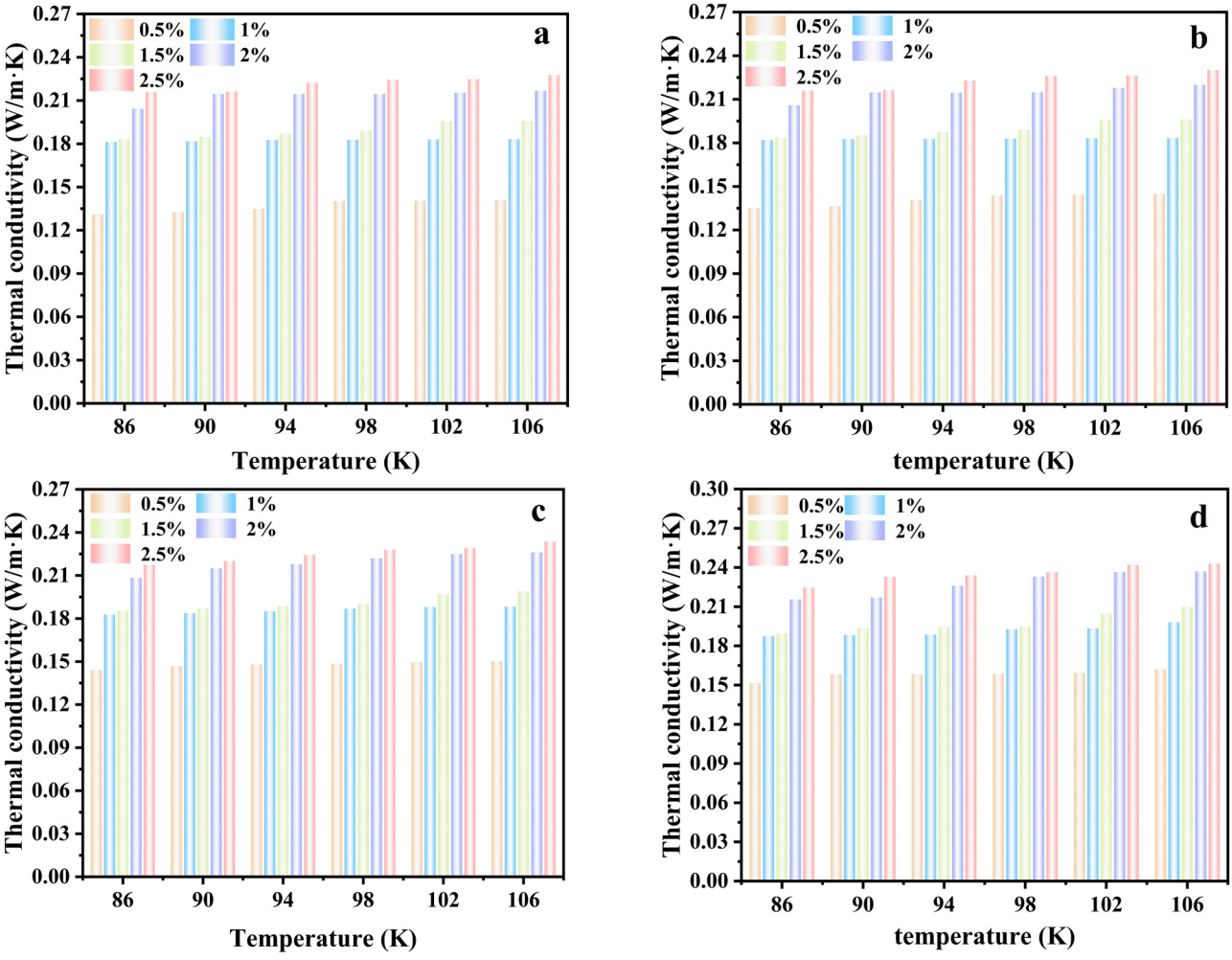

Figure 10: Variation patterns of thermal conductivity in Al–Ar nanofluids with volume fraction. (a) Cylinder, (b) sphere, (c) cube, and (d) platelets.

It is observed from the figures that the thermal conductivity of nanofluids steadily increases with the rise in volume fraction. The maximum thermal conductivity values for each NP shape occur at a volume fraction of 2.5% and a temperature of 106 K, specifically: 0.22766 W/m K (2.5%, 106 K, cylinder), 0.23 W/m K (2.5%, 106 K, sphere), 0.2336 W/m K (2.5%, 106 K, cube), and 0.243 W/m K (2.5%, 106 K, platelets). The increase in nanofluid thermal conductivity with the increase in NP volume fraction is mainly attributed to the amplification of the interface NP ball effect due to the increased concentration of NPs, leading to enhanced thermal conductivity of the nanofluid [60]. The conclusion of this study further demonstrates that the increase in nanofluid thermal conductivity due to the increase in NP volume fraction is primarily attributed to the NP ball effect rather than the Brownian motion effect [54], which is distinct from the increase observed with elevated temperature, aligning with previous research findings [61,62].

The study results investigating the influence of different volume fractions of NPs on the viscosity of Al–Ar nanofluids are presented in the form of a bar graph in Figure 11. From Figure 11(a–d), it is evident that the viscosity of Al–Ar nanofluids increases with the rise in NP volume fraction. For each NP shape condition, the maximum and minimum viscosity values are as follows: cylinder shape: the maximum viscosity is 0.00046923 Pa S (2.5%, 86 K), and the minimum viscosity is 0.0002523 Pa S (0.5%, 106 K). Sphere shape: the maximum viscosity is 0.00046499 Pa S (2.5%, 86 K), and the minimum viscosity is 0.000230161 Pa S (0.5%, 106 K). Cube shape: the maximum viscosity is 0.000477 Pa S (2.5%, 86 K), and the minimum viscosity is 0.000208 Pa S (0.5%, 106 K). Platelet shape: the maximum viscosity is 0.0004882 Pa

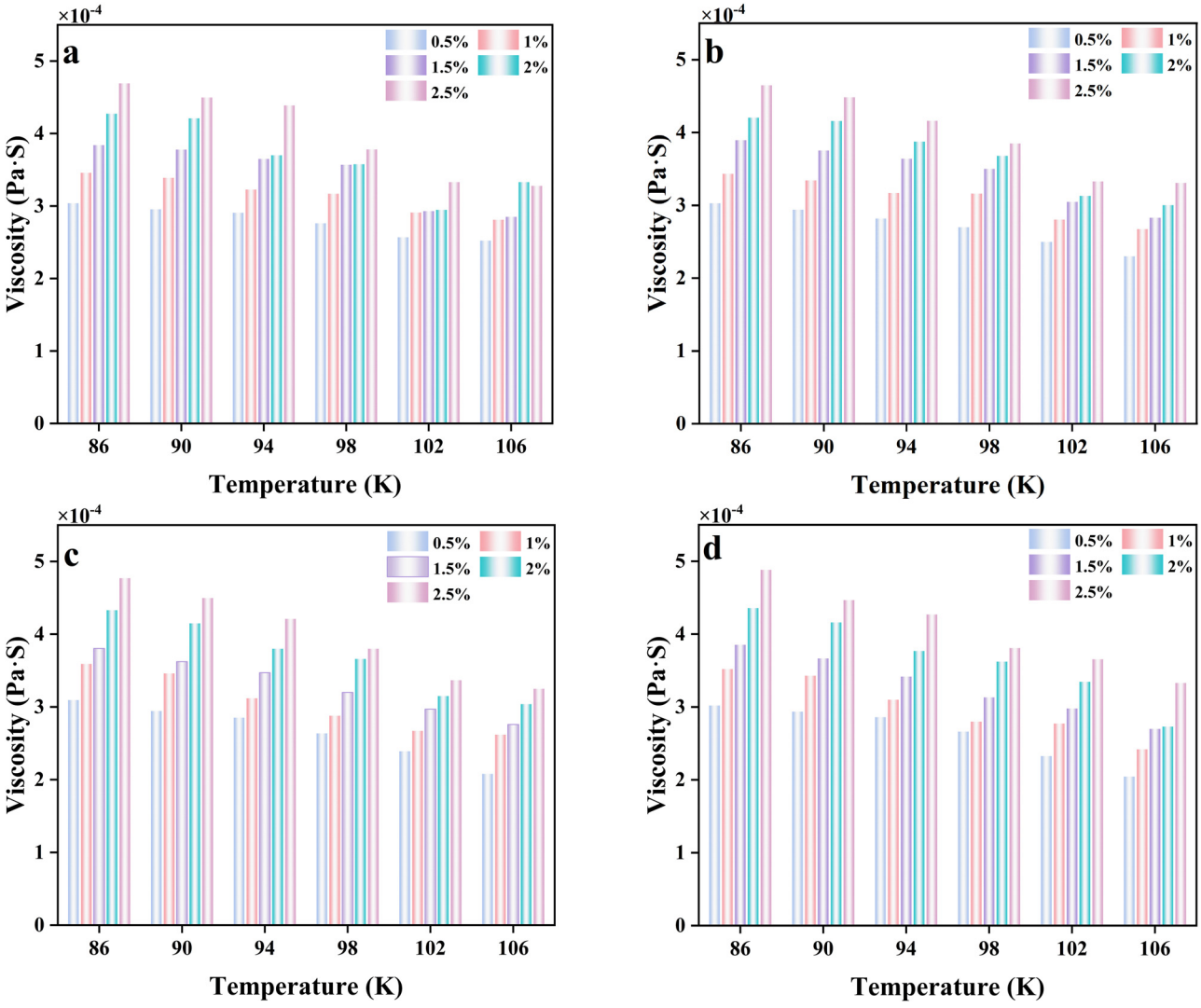

Figure 11: Variation trends of viscosity in Al–Ar nanofluids with volume fraction. (a) Cylinder, (b) sphere, (c) cube, and (d) platelets.

S (2.5%, 86 K), and the minimum viscosity is 0.0002045 Pa S (0.5%, 106 K).

In contrast to the significant increase in thermal conductivity with an increase in NP volume fraction, viscosity steadily rises with the increase in NP volume fraction. These results indicate that NP volume fraction is a crucial factor influencing nanofluid viscosity, particularly due to the formation of an ordered liquid layer at the solid–liquid interface between NPs and the BF [43]. Specifically, the stronger interaction between Ar atoms and metal atoms in the nanofluid leads to a higher attraction of Ar atoms by metal NPs, resulting in the formation of an ordered liquid layer at the interface between the liquid and metal NPs. This phenomenon significantly increases the effective volume fraction of NPs in the nanofluid, ultimately leading to an increase in viscosity [63].

3.3 Effect of NP shape and temperature on thermal conductivity and viscosity in Al_2O_3–Ar nanofluids

This section investigates the influence of four different NP shapes – cylinder, sphere, cube, and platelets – and varying temperatures on the thermal conductivity and viscosity of Al_2O_3–Ar nanofluids.

We present the study findings on the impact of NP shape and temperature on the thermal conductivity of Al_2O_3–Ar nanofluids in the form of 3D surface plots in Figure 12. Figure 12(a–e) visually depicts that the thermal conductivity of Al_2O_3–Ar nanofluids increases with temperature, and nanofluids formed by NPs with higher shape factors (S/V values) exhibit higher thermal conductivity. The nanofluid with platelet-shaped NPs at 106 K, where the S/V value is maximum (0.805), shows the highest thermal conductivity for each volume fraction, with values of 0.1573 W/m K (0.5%, 106 K, platelets), 0.1973 W/m K (1%, 106 K, platelets), 0.2075 W/m K (1.5%, 106 K, platelets), 0.234 W/m K (2%, 106 K, platelets), and 0.2366 W/m K (2.5%, 106 K, platelets).

The observed increase in thermal conductivity of Al_2O_3–Ar nanofluids with rising temperature aligns with previous research findings. This consistency with the trends in thermal conductivity observed in Section 3.1 for Al–Ar nanofluids indicates the scientific reliability of these results. Furthermore, the internal mechanisms leading to this outcome align with those discussed in detail in Section 3.1 for the thermal conductivity trend of Al–Ar nanofluids with temperature. The increased intensity of Brownian motion of NPs in nanofluids leads to faster internal heat transfer efficiency, thereby exhibiting higher thermal conductivity of nanofluids [52]. Moreover, the degree of Brownian motion of NPs in nanofluids increases with temperature, resulting in an increase in thermal conductivity of nanofluids with increasing environmental temperature [53].

Regarding the shape factor (S/V value), we observed that the influence of S/V value on the thermal conductivity of Al_2O_3–Ar nanofluids follows a pattern similar to its effect on Al–Ar nanofluids. Specifically, the thermal conductivity of Al_2O_3–Ar nanofluids increases with the augmentation of the S/V value. We calculated the growth rates of thermal conductivity relative to pure Ar fluid for Al_2O_3–Ar nanofluids with a volume fraction of 0.5% at a temperature of 106 K. The results are as follows: 4.6% (cylinder, S/V = 0.31746), 11.6% (sphere, S/V = 0.357), 16.1% (cube, S/V = 0.441176), and 21.9% (platelets, S/V = 0.805). These findings indicate that the growth rate of thermal conductivity in Al_2O_3–Ar nanofluids increases with the rise of S/V values. This trend is consistent with the observed behavior in Al–Ar nanofluids. Additionally, the internal mechanisms leading to this outcome align with those discussed in detail in Section 3.1 for the thermal conductivity trend of Al–Ar nanofluids with temperature. The crucial role of NP surface area in the thermal conductivity of nanofluids [55] is primarily attributed to the different shapes (S/V ratio) of NPs, resulting in various surface effects [54], hence leading to different thermal conductivities of nanofluids with different shapes (S/V ratio) of NPs. Additionally, it was found in the study that the criterion for determining the extent to which the thermal conductivity of nanofluids is affected by NPs is the ratio of energy atoms in NPs, denoted as E. As the S/V ratio of NPs increases, E also increases [56]. Therefore, in this study, the growth rate of thermal conductivity of nanofluids increases with the increase in the S/V ratio of NPs.

We present the research results of NP shape and temperature effects on the viscosity of Al_2O_3–Ar nanofluids in the form of bar graphs in Figure 13. From Figure 13(a–e), it is visually evident that the viscosity of Al_2O_3–Ar nanofluids decreases with an increase in temperature. The influence of NP shape on the viscosity of Al–Ar nanofluids is relatively small. For each volume fraction, the highest and lowest viscosity values are as follows: when the NP volume fraction is 0.5%, the highest value is 0.006891 Pa S (0.5%, 86 K, cylinder), and the lowest value is 0.0041 Pa S (0.5%, 106 K, sphere). When the NP volume fraction is 1%, the highest value is 0.007462 Pa S (1%, 86 K, cylinder), and the lowest value is 0.00541 Pa S (1%, 106 K, sphere). When the NP volume fraction is 1.5%, the highest value is 0.00809 Pa S (1.5%, 86 K, cube), and the lowest value is 0.00626 Pa S (1.5%, 106 K, sphere). When the NP volume fraction is 2%, the highest value is 0.008387 Pa S (2%, 86 K, platelets), and the lowest value is

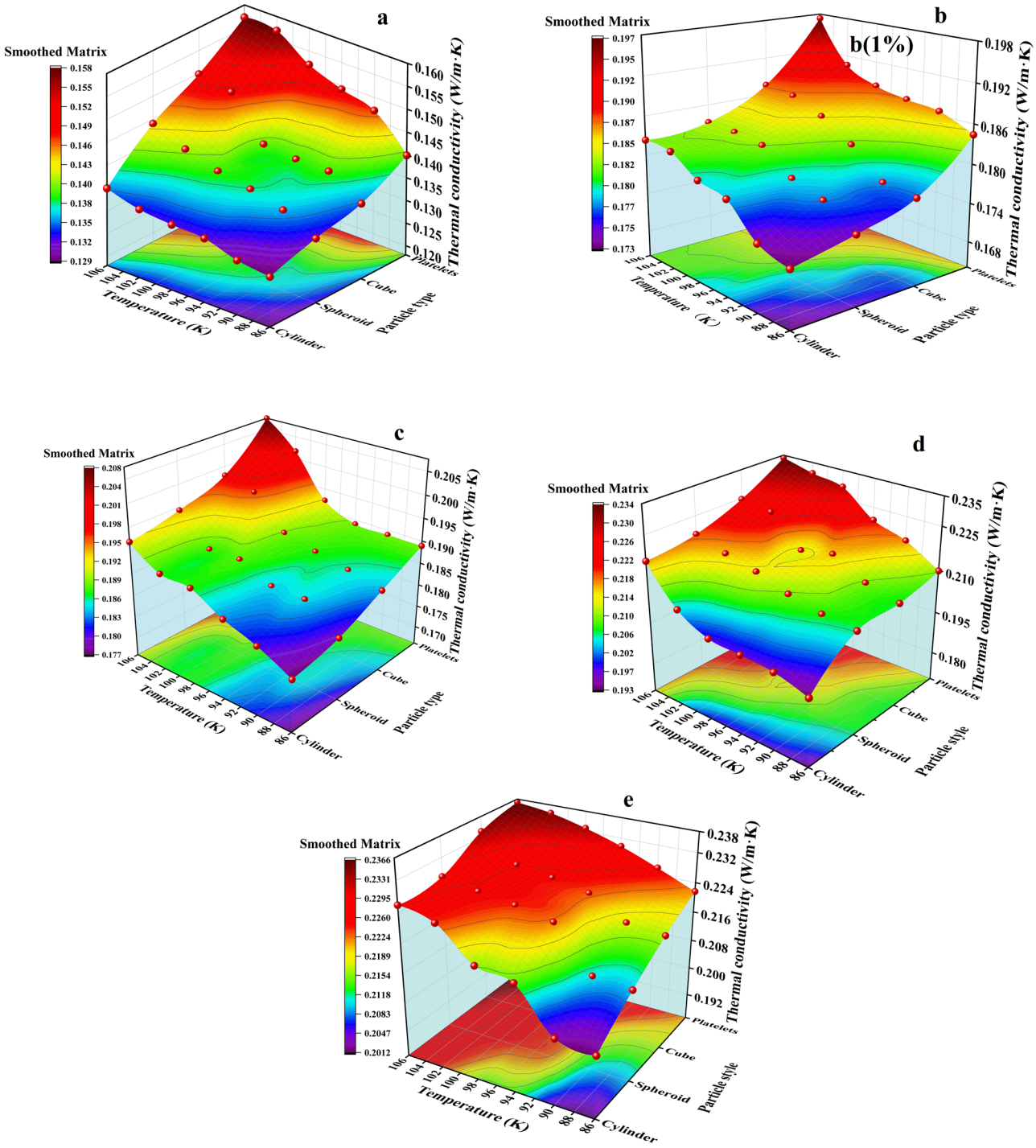

Figure 12: Variation trends of thermal conductivity in Al_2O_3–Ar nanofluids with temperature and shape factor (*S*/*V* value). (a) 0.5%, (b) 1%, (c) 1.5%, (d) 2%, (e) 2.5%.

0.0071 Pa S (2%, 106 K, sphere). When the NP volume fraction is 2.5%, the highest value is 0.008975 Pa S (2.5%, 86 K, platelets), and the lowest value is 0.007355 Pa S (2.5%, 86 K, cube). The results indicate that the viscosity of Al_2O_3–Ar nanofluids decreases with an increase in temperature, which is consistent with the trend observed in the viscosity of Al–Ar nanofluids. Additionally, the internal mechanism leading to this result aligns with the internal mechanism of viscosity variation with temperature observed in Al–Ar nanofluids. Since the adhesive forces within the fluid

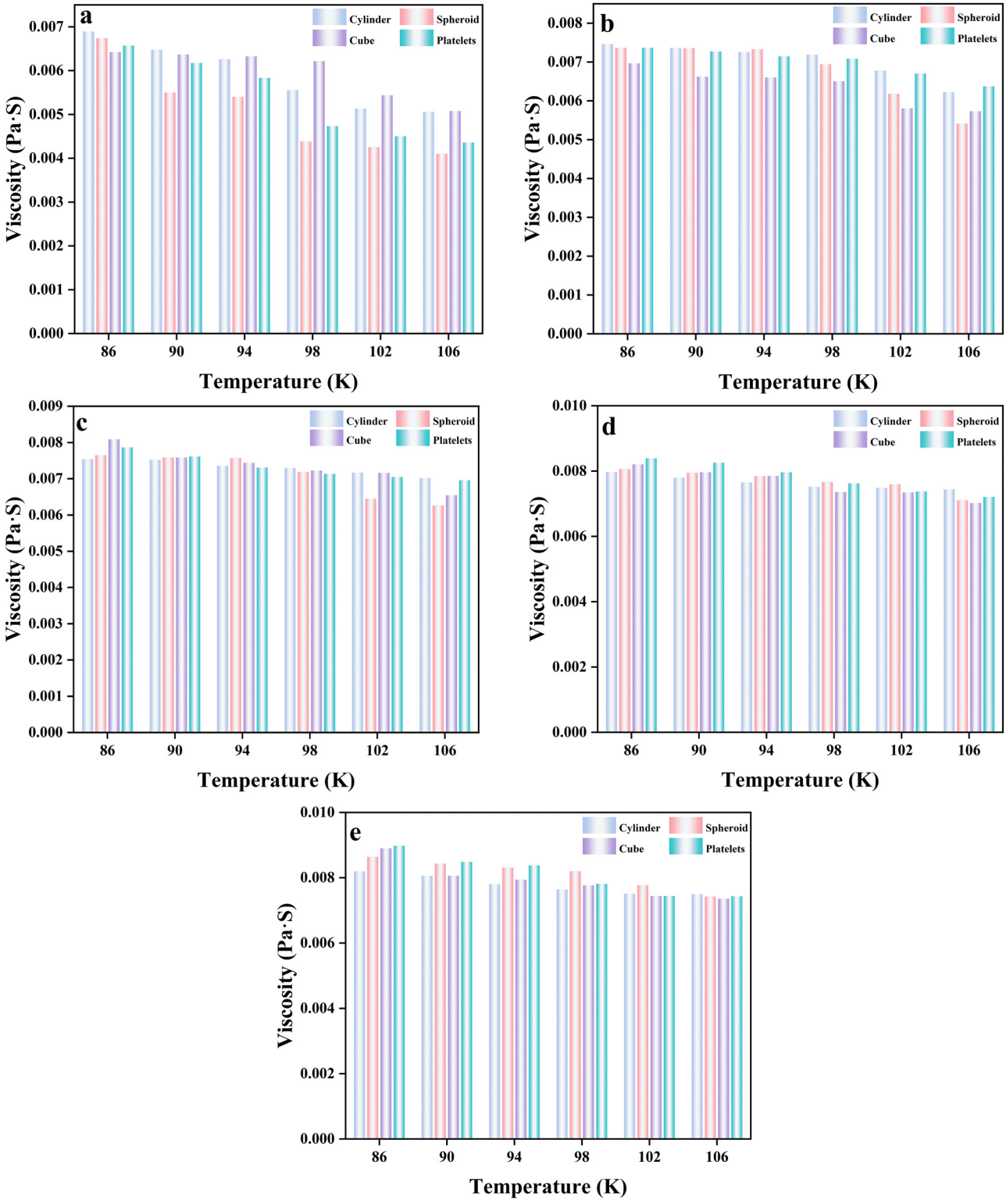

Figure 13: Variation trends of viscosity in Al_2O_3–Ar nanofluids with temperature and shape factor (*S*/*V* value). (a) 0.5%, (b) 1%, (c) 1.5%, (d) 2%, (e) 2.5%.

are overcome by the thermal energy of fluid molecules, the viscosity of the fluid decreases with increasing temperature. Moreover, the gaps between the BF and NPs in nanofluids increase with temperature, reducing the resistance to nanofluid flow and thus decreasing its viscosity [59].

3.4 Effect of NP volume fraction on the thermal conductivity and viscosity of Al_2O_3–Ar nanofluid

In this section, the impact of NPs with different volume fractions and shapes on the thermal conductivity and viscosity of Al_2O_3–Ar nanofluid is investigated. Similar to the previous section, the NP shapes considered are cylinder, sphere, cube, and platelets.

The research results on the influence of different volume fractions of NPs on the thermal conductivity of Al_2O_3–Ar nanofluid are presented in bar charts in Figure 14. Figure 14(a–f)

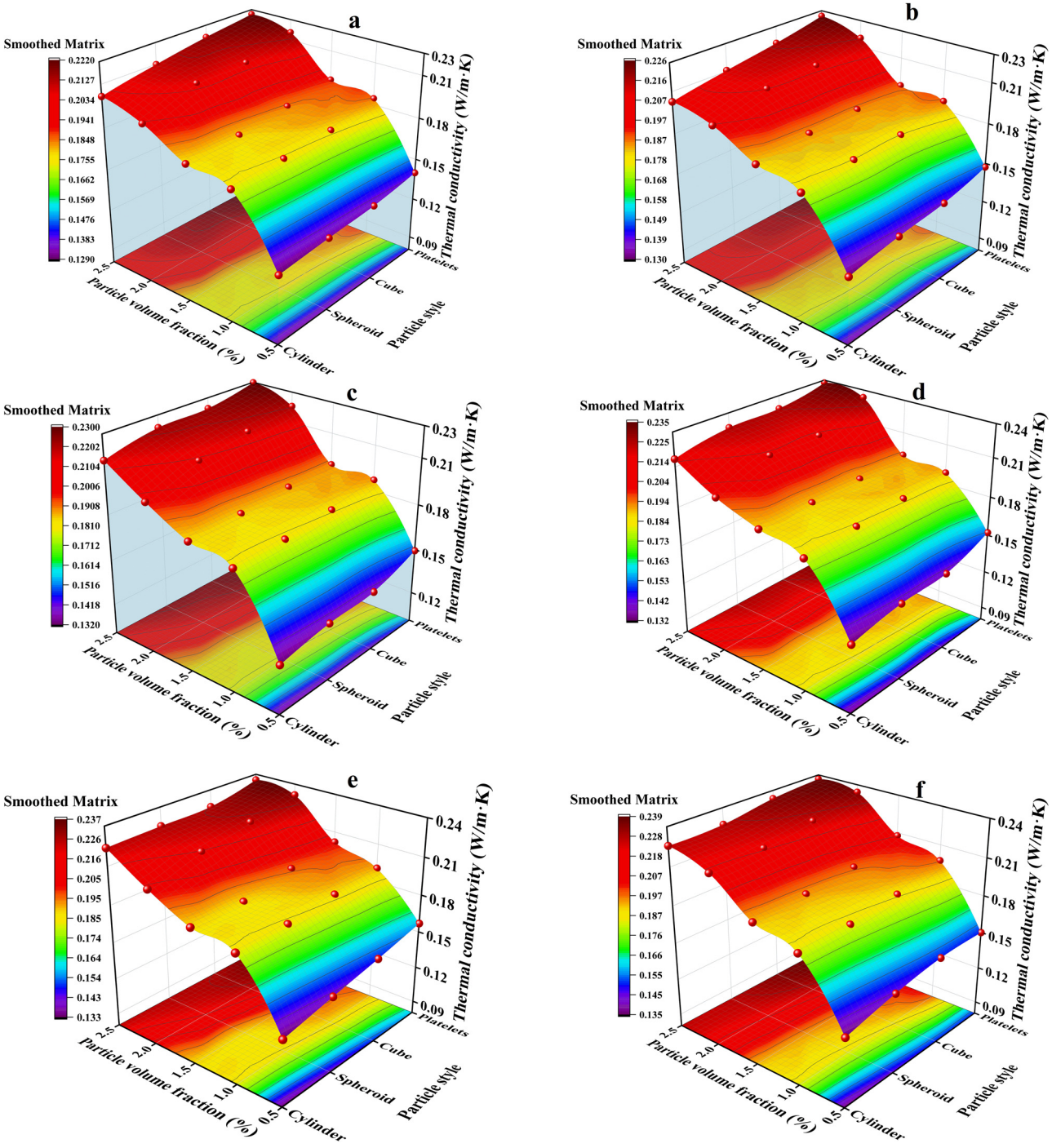

Figure 14: Variation trend of thermal conductivity with NP volume fraction in Al_2O_3–Ar nanofluid. (a) 86 K, (b) 90 K, (c) 94 K, (d) 98 K, (e) 102 K, and (f) 106 K.

visually demonstrates the variation of Al_2O_3–Ar nanofluid thermal conductivity with volume fraction and temperature. While the previous section discussed the temperature-dependent behavior, this section emphasizes the variation trend with volume fraction. It is observed that the thermal conductivity of the nanofluid steadily increases with the rise in NP volume fraction. The maximum thermal conductivity for each NP shape is achieved at a volume fraction of 2.5% and a temperature of 106 K, with values of 0.2259 W/m K (cylinder), 0.227 W/m K (sphere), 0.2335 W/m K (cube), and 0.2366 W/m K (platelets).

The results indicate that the thermal conductivity of Al_2O_3–Ar nanofluid increases with the growth of NP volume fraction, exhibiting a similar trend to the findings for Al–Ar nanofluid. Moreover, the internal mechanisms causing this outcome align with the internal mechanisms governing the variation of thermal conductivity with NP volume fraction in Al–Ar nanofluid. The main reason is that the interface NP clustering effect of nanofluids amplifies with increasing NP concentration, leading to an enhancement in thermal conductivity [60]. The conclusions of this study further demonstrate that unlike the increase in thermal conductivity of nanofluids due to temperature elevation, the primary reason for the increase in thermal conductivity with the increase in NP volume fraction is the NP clustering effect rather than the Brownian motion effect [54,61,62].

The research results on the impact of different volume fractions of NPs on the viscosity of Al_2O_3–Ar nanofluid are presented in the form of bar charts (Figure 15(a–d)). The charts provide a visual representation showing that the viscosity of Al_2O_3–Ar nanofluid increases with the rise in NP volume fraction. For each NP shape condition, the maximum and minimum viscosity values are as follows: for cylindrical NPs: the maximum viscosity is 0.008192 Pa S (2.5%, 86 K), and the minimum viscosity is 0.005057 Pa S (0.5%, 106 K). For spherical NPs: the maximum viscosity

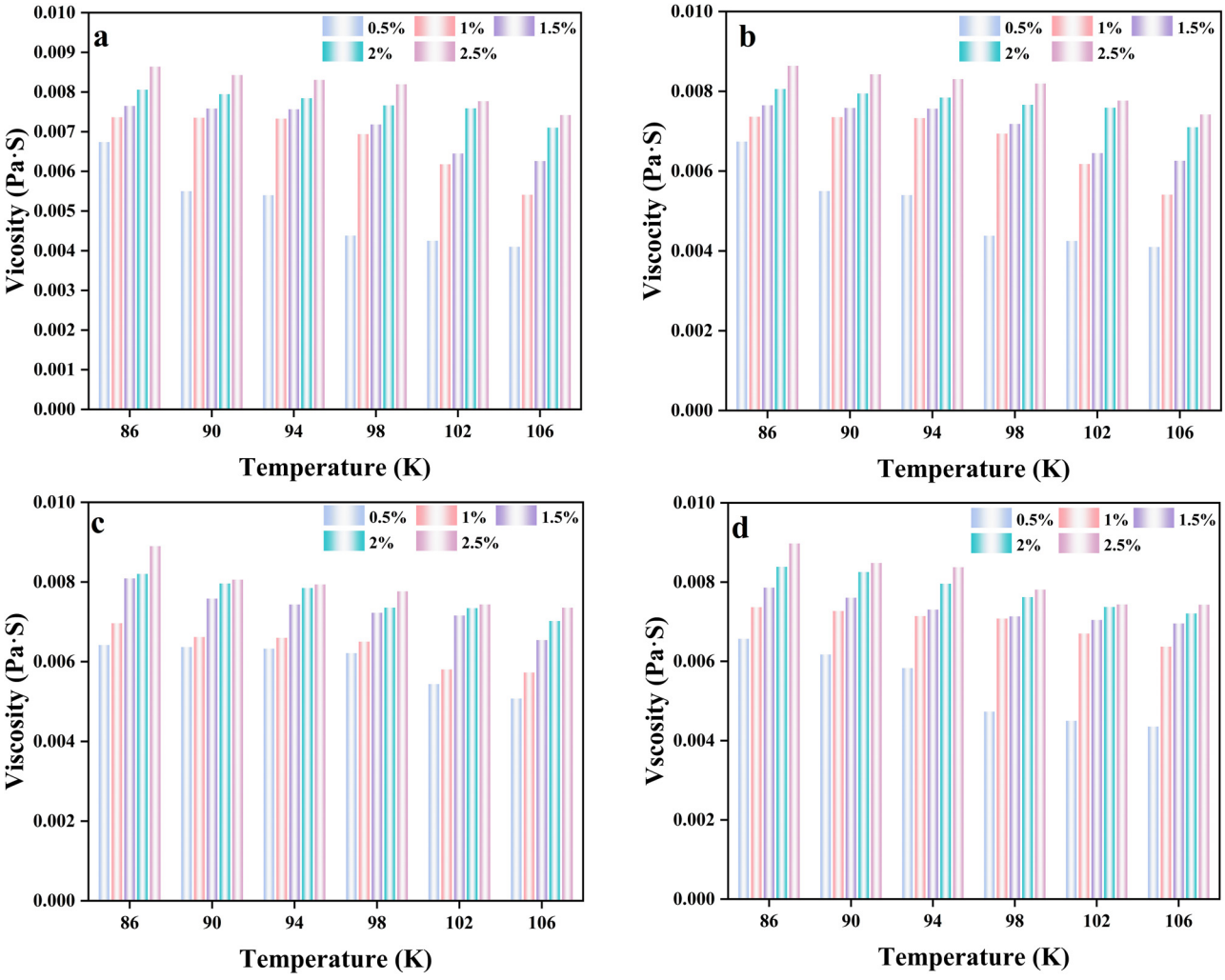

Figure 15: Variation pattern of viscosity in Al_2O_3–Ar nanofluid with respect to volume fraction. (a) Cylinder, (b) sphere, (c) cube, and (d) platelets.

is 0.00864 Pa S (2.5%, 86 K), and the minimum viscosity is 0.0041 Pa S (0.5%, 106 K). For cubic NPs: the maximum viscosity is 0.0088996 Pa S (2.5%, 86 K), and the minimum viscosity is 0.005076 Pa S (0.5%, 106 K). For platelet-shaped NPs: the maximum viscosity is 0.008975 Pa S (2.5%, 86 K), and the minimum viscosity is 0.004356 Pa S (0.5%, 106 K).

Unlike the sharp increase observed in thermal conductivity with the increase in NP volume fraction, viscosity steadily rises as the NP volume fraction increases. This study aligns with the trends observed in the influence of NP volume fraction on the viscosity of Al–Ar nanofluid. The internal mechanisms leading to these results are consistent with the internal mechanisms governing the viscosity of Al–Ar nanofluid with varying NP volume fractions. This is associated with the solid-like liquid layer at the interface between the base liquid and NPs in nanofluids [43], specifically because the interaction between the base liquid atoms (Ar atoms) and the metal atoms is stronger than their interaction with their own atoms (Ar atoms), resulting in the formation of an ordered liquid layer at the interface between the liquid and metal NPs. This leads to a significant increase in the effective volume fraction of NPs in the nanofluid, ultimately resulting in an increase in viscosity [63].

3.5 Comparison of thermal conductivity between Al–Ar nanofluid and Al_2O_3–Ar nanofluid

In this section, a comparative analysis of the thermal conductivity of Al–Ar nanofluid and Al_2O_3–Ar nanofluid is conducted from the perspectives of temperature, shape, and volume fraction. The research results, depicted in Figures 16 and 17, showcase the thermal conductivity of nanofluids formed by both metal and metal oxide NPs in the same type of BF, considering variations in temperature, shape factors (S/V ratio), and volume fractions.

As observed from Figures 16 and 17, and in alignment with the conclusions drawn in previous sections, it is evident that the thermal conductivity of both Al–Ar nanofluid and Al_2O_3–Ar nanofluid increases with rising temperature. Additionally, the conductivity rises with higher shape factors (S/V ratios), and the growth rate of conductivity is directly proportional to the increase in S/V ratio. Furthermore, both nanofluids exhibit an increase in thermal conductivity with higher volume fractions.

While sharing these common characteristics, this study reveals that there exists a numerical difference in the thermal conductivity of nanofluids formed by metal and metal oxide NPs in the same type of BF. In general, nanofluids formed by metal NPs demonstrate higher thermal conductivity compared to those formed by their metal oxide counterparts in the same type of BF.

For instance, at a volume fraction of 1.5% and with cylindrical-shaped NPs, the thermal conductivity of Al–Ar nanofluid and Al_2O_3–Ar nanofluid is as follows: Al–Ar: 0.1832 W/m K (1.5%, cylinder, 86 K), 0.1847 W/m K (1.5%, cylinder, 90 K), 0.1871 W/m K (1.5%, cylinder, 94 K), 0.18886 W/m K (1.5%, cylinder, 98 K), 0.19549 W/m K (1.5%, cylinder, 102 K), 0.19579 W/m K (1.5%, cylinder, 106 K). Al_2O_3–Ar: 0.17745 W/m K (1.5%, cylinder, 86 K), 0.1811 W/m K (1.5%, cylinder, 90 K), 0.1836 W/m K (1.5%, cylinder, 94 K), 0.1873 W/m K (1.5%, cylinder, 98 K), 0.1876 W/m K (1.5%, cylinder, 102 K), and 0.1919 W/m K (1.5%, cylinder, 102 K). In our study, we compared our findings with existing research results. Milanese *et al.* [64] discussed the stratification phenomena in nanofluids, noting the differences in thermal conductivity between Cu–H_2O and CuO–H_2O. Their simulation and experimental results closely align with ours, indicating that nanofluids composed of metals have higher thermal conductivity than those composed of the same metals' oxides mixed with the same type of BF.

Similarly, Jamal-Abad *et al.* [65] examined the thermal conductivity of Al–H_2O nanofluids, Ruvo *et al.* [66] investigated the thermal conductivity of Al_2O_3–H_2O nanofluids using a mathematical model, while El Hadoui and Kaddiri [67] employed the lattice Boltzmann method combined with volume fraction to study the thermal conductivity and viscosity of Al_2O_3–H_2O nanofluids, and Huang *et al.* [68] studied the thermal conductivity of Al_2O_3–H_2O nanofluids. Comparing their findings with ours provides a robust analogy. Furthermore, Liu *et al.* [51] investigated the thermal conductivity of Al–Ar nanofluids, and their results match ours very well.

These comparisons with current studies demonstrate the scientific reliability and validity of our results.

This study provides a comprehensive analysis of the results depicted in Figures 16 and 17. The observed differences in thermal conductivity between nanofluids formed by metal and metal oxide NPs in the same type of BF are attributed to variations in interfacial thermal conduction. A detailed examination, utilizing PDOS, was conducted to investigate this phenomenon. Given that all results in this study consistently show higher thermal conductivity for Al–Ar nanofluid compared to Al_2O_3–Ar nanofluid, we randomly selected six data points for PDOS calculations. These points include cylindrical-shaped NPs at 2.5% volume fraction and 86 K, plate-shaped NPs at 0.5% volume fraction and 90 K, cube-shaped NPs at 0.5% volume fraction and 94 K, cylindrical-shaped NPs at 2% volume fraction and

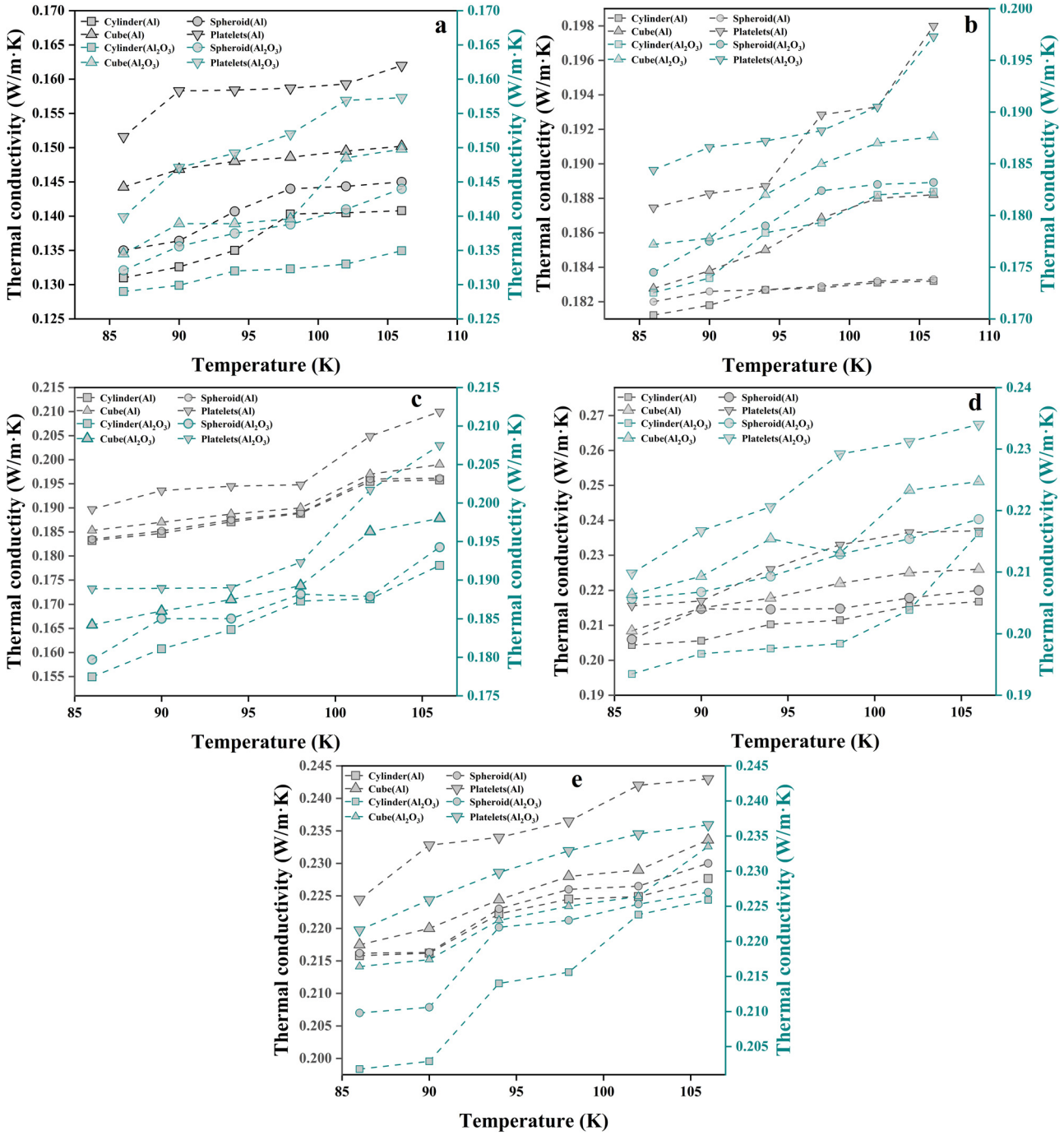

Figure 16: Disparities and similarities in thermal conductivity between Al–Ar nanofluid and Al_2O_3–Ar nanofluid under constant volume fraction with varied temperature and NP shape factor (*S*/*V* ratio). (a) 0.5%, (b) 1%, (c) 1.5%, (d) 2%, (e) 2.5%.

94 K, spherical-shaped NPs at 1.5% volume fraction and 102 K, and plate-shaped NPs at 2% volume fraction and 106 K.

The overlap between the PDOS curves for Al and Ar, as well as Al_2O_3 and Ar, was observed at these data points, as shown in Figure 18. Higher overlap indicates the increased interfacial thermal conduction, consequently resulting in higher thermal conductivity for the entire nanofluid system [69]. Figure 18(a–f) demonstrates that the overlap between Al and Ar PDOS is greater than that between Al_2O_3 and Ar. To quantify this conclusion, a code was developed to calculate the percentage of overlap between the PDOS curves, and MATLAB was employed for computation. The results for the six data points are as follows: 99.991% overlap at

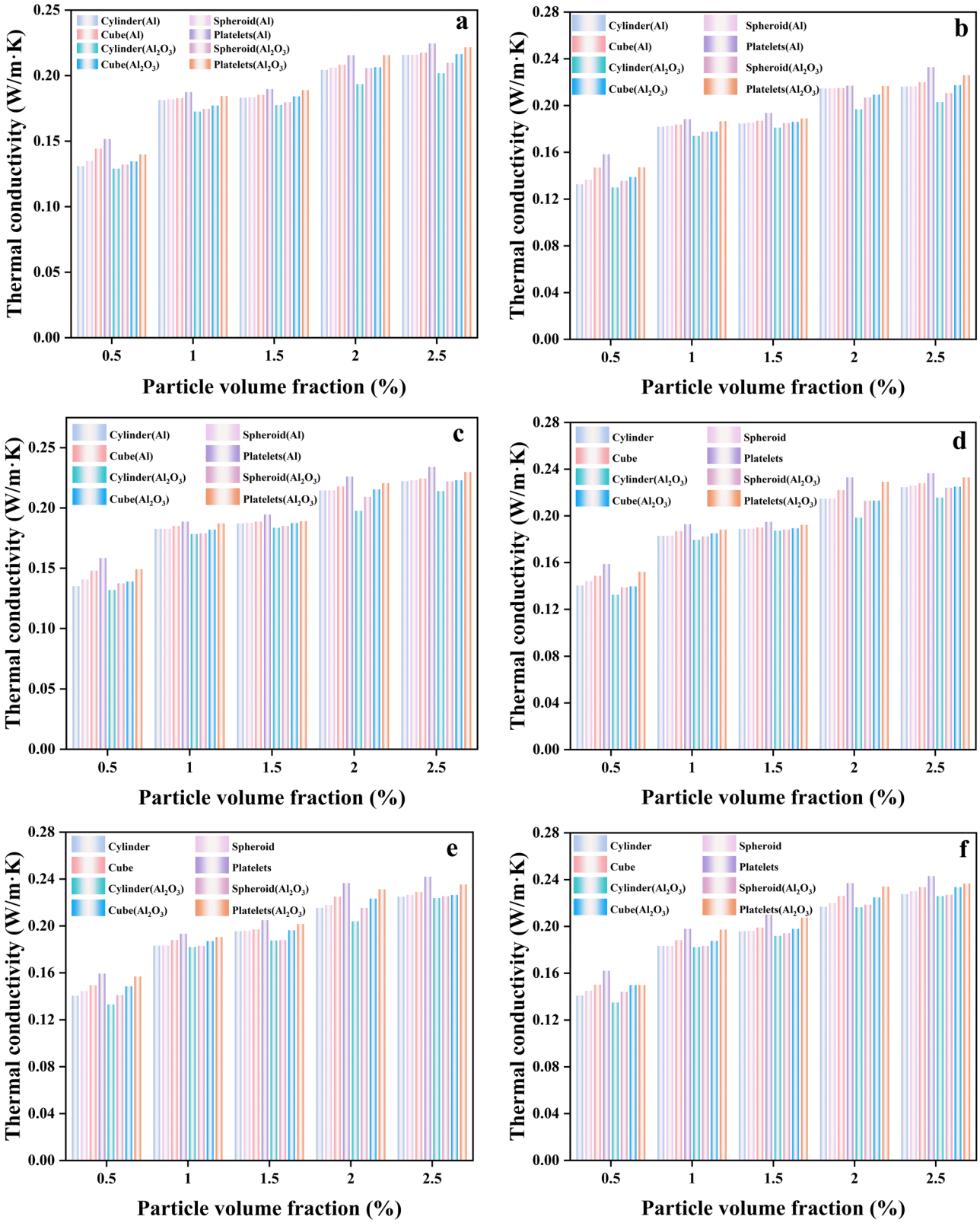

Figure 17: Disparities and similarities in thermal conductivity between Al–Ar nanofluid and Al_2O_3–Ar nanofluid under constant temperature with varied volume fraction and NP shape. (a) 86 K, (b) 90 K, (c) 94 K, (d) 98 K, (e) 102 K, and (f) 106 K.

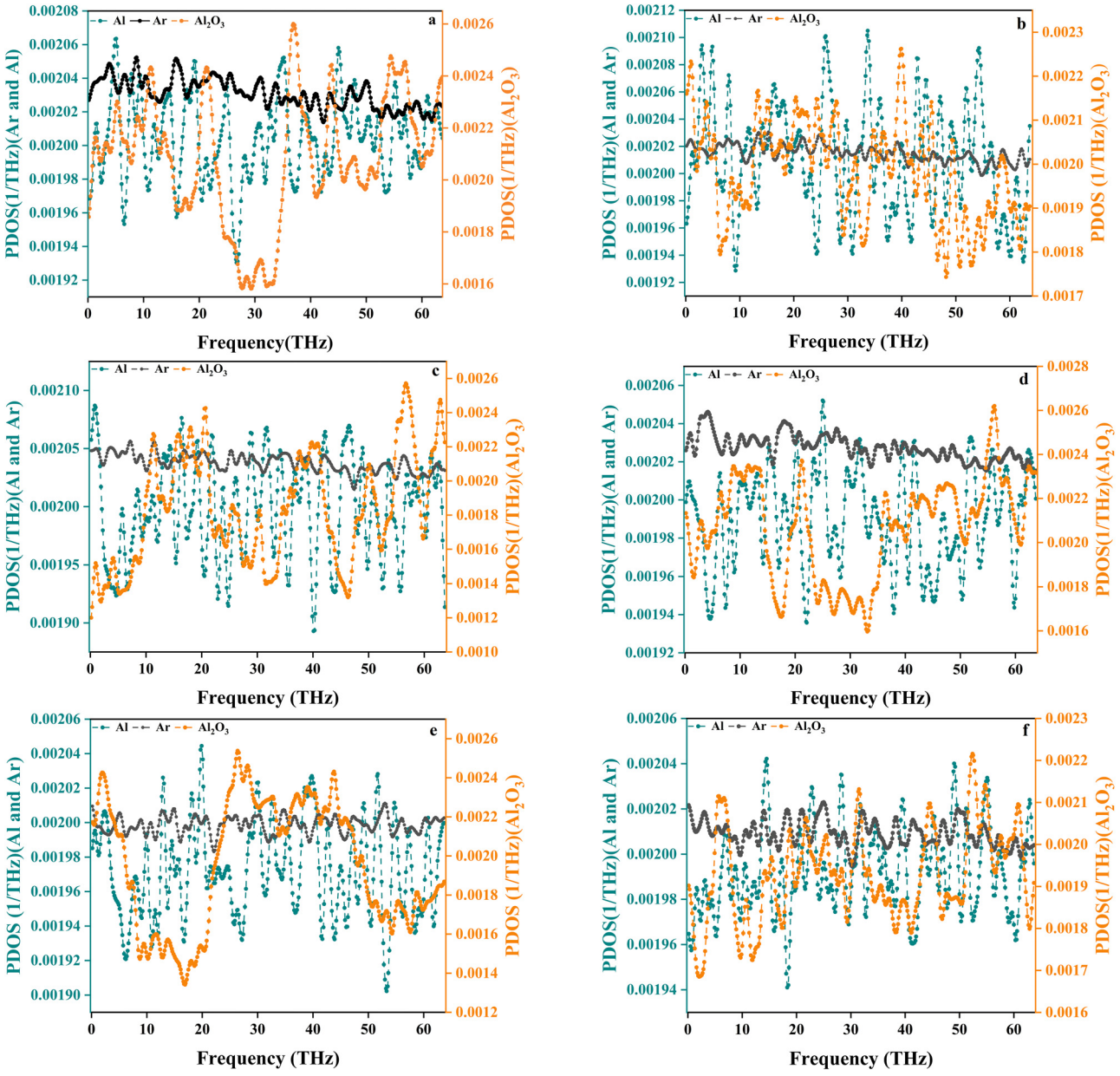

Figure 18: Comparative PDOS curves for Al, Ar, and Al_2O_3 in nanofluids under varied temperature, volume fraction, and NP shape conditions. (a) 86 K 2.5% cylinder, (b) 90 K 0.5% platelets, (c) 94 K 0.5% cube, (d) 94 K 2% cylinder, (e) 102 K 1.5% sphere, and (f) 106 K 2% platelets.

86 K, 2.5%, platelets (Al and Ar), 99.313% at 86 K, 2.5%, platelets (Al_2O_3 and Ar); 99.98% at 90 K, 0.5%, platelets (Al and Ar), 99.847% at 90 K, 0.5%, platelets (Al_2O_3 and Ar); 99.976% at 94 K, 0.5%, cube (Al and Ar), 98.477% at 94 K, 0.5%, cube (Al_2O_3 and Ar); 99.991% at 94 K, 2%, cylinder (Al and Ar), 99.406% at 94 K, 2%, cylinder (Al_2O_3 and Ar); 99.99% at 102 K, 1.5%, sphere (Al and Ar), 98.641% at 102 K, 1.5%, sphere (Al_2O_3 and Ar); 99.995% at 106 K, 2%, platelets (Al and Ar); and 99.837% at 106 K, 2%, platelets (Al_2O_3 and Ar).

The consistent observation across all data points is that the overlap percentage for Al and Ar is greater than that for Al_2O_3 and Ar. This deeper-level analysis from the perspectives of phonon transport and interfacial thermal conduction explains the obtained result in this study, where the thermal conductivity of Al–Ar nanofluid is higher than that of Al_2O_3–Ar nanofluid.

In this study, we have used the degree of overlap of the areas enclosed by the PDOS curves of different types of atoms with the coordinate axes to explain the differences in thermal conductivity of nanofluids from a microscopic perspective. The order of the PDOS overlap closely matches the order of thermal conductivities observed in our

nanofluids. This method of using PDOS overlap to compare thermal conductivities has also been employed in other studies. For example, Jin *et al.* [36] investigated the thermal conductivity of nanofluids composed of different metal NPs and calculated the PDOS overlap for these nanofluids. They found that nanofluids with greater PDOS overlap exhibit higher thermal conductivities, which corroborates the reliability and scientific validity of our results.

3.6 Contrastive analysis of viscosity between Al–Ar nanofluid and Al_2O_3–Ar nanofluid

In this section, a meticulous comparison of viscosity is conducted between Al–Ar nanofluid and Al_2O_3–Ar nanofluid, focusing on temperature, shape, and volume fraction. The viscosity research results comparing the nanofluid formed with a metal and the nanofluid formed with the

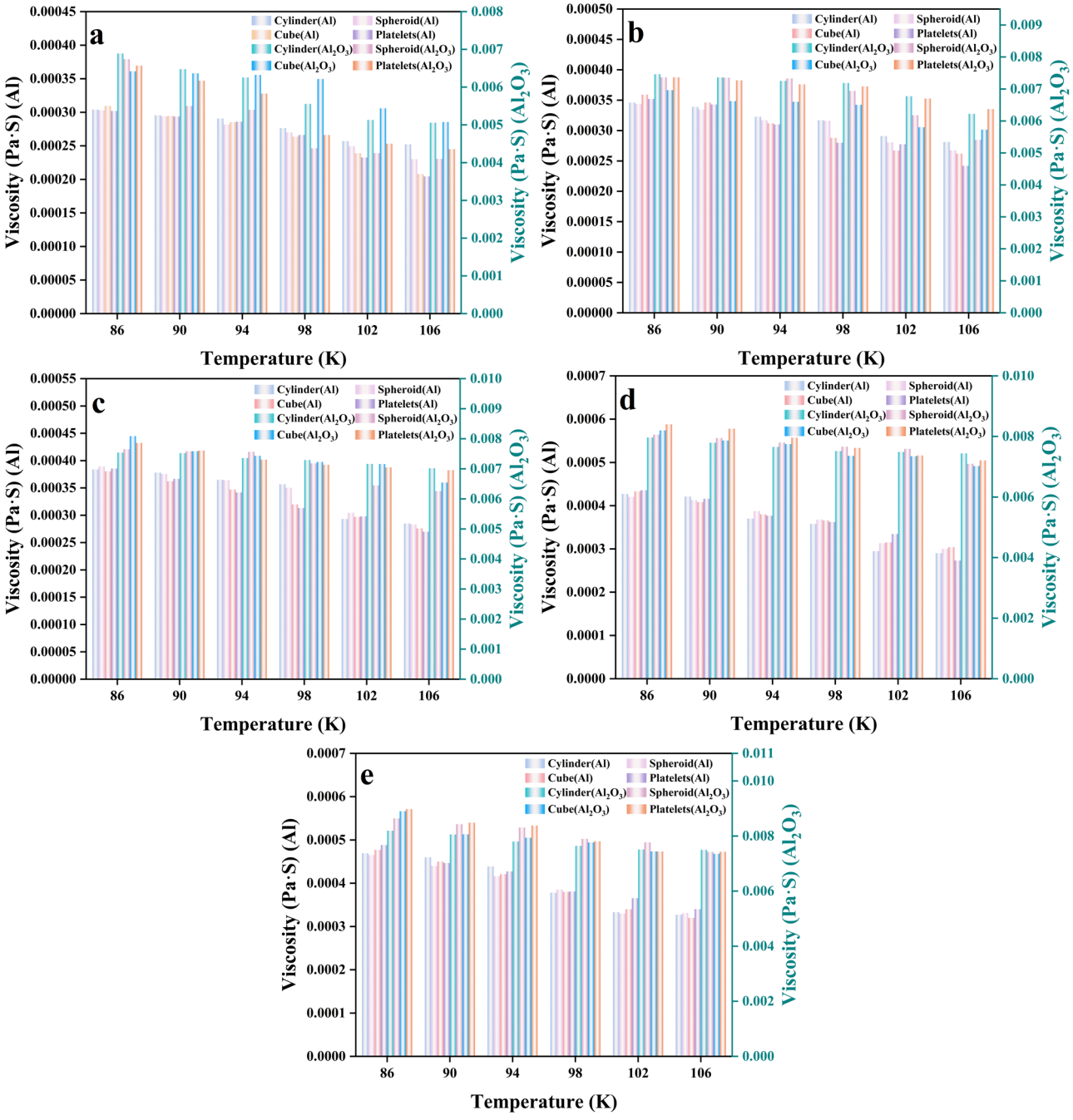

Figure 19: Viscosity of Al–Ar nanofluid and Al_2O_3–Ar nanofluid under variations in temperature and NP shape factor (*S*/*V* value) at a constant NP volume fraction. (a) 0.5%, (b) 1%, (c) 1.5%, (d) 2%, (e) 2.5%.

oxide of this metal under temperature and shape variations are shown in Figure 19. Similarly, the viscosity research results comparing the nanofluid formed with a metal and the nanofluid formed with the oxide of this metal under variations in NP volume fraction are shown in Figure 20.

From Figures 19 and 20, and the conclusions drawn in the preceding sections, it is evident that the viscosity of both Al–Ar nanofluid and Al_2O_3–Ar nanofluid decreases with an increase in temperature, increases with an increase in volume fraction, and exhibits a minimal variation with changes in nanofluid particle shape (S/V ratio). Beyond these similarities, this study also observes numerical differences in viscosity between nanofluid formed with a metal and the nanofluid formed with the oxide of this metal. Generally, nanofluids formed with metallic NPs exhibit lower viscosity compared to nanofluids formed with their oxide counterparts. This research outcome is visually demonstrated in Figures 19 and 20.

To exemplify, six data points are extracted from all data for illustration: 0.0004882 Pa S (Al–Ar nanofluid, 86 K, 2.5%, platelets), 0.008975 Pa S (Al_2O_3–Ar nanofluid, 86 K, 2.5%, platelets); 0.0002936 Pa S (Al–Ar nanofluid, 90 K, 0.5%, platelets), 0.006173 Pa S (Al_2O_3–Ar nanofluid, 90 K, 0.5%, platelets); 0.0002852 Pa S (Al–Ar nanofluid, 94 K, 0.5%, cube), 0.005832 Pa S (Al_2O_3–Ar nanofluid, 94 K, 0.5%, cube); 0.00037 Pa S (Al–Ar nanofluid, 94 K, 2%, cylinder), 0.007652 Pa S (Al_2O_3–Ar nanofluid, 94 K, 2%, cylinder); 0.0003047 Pa S (Al–Ar nanofluid, 102 K, 1.5%, sphere), 0.00645 Pa S (Al_2O_3–Ar nanofluid, 102 K, 1.5%, sphere); 0.0002731 Pa S (Al–Ar nanofluid, 106 K, 2%, platelets), 0.00721 Pa S (Al_2O_3–Ar nanofluid, 106 K, 2%, platelets). All the data points indicate that nanofluids formed with metallic NPs have lower viscosity than those formed with their oxide counterparts. This is attributed to the more complex internal structure of metal oxides compared to metals, resulting in a larger internal surface area. Consequently, metal oxide nanofluids exhibit higher viscosity than metal nanofluids due to stronger interactions with BF molecules [59].

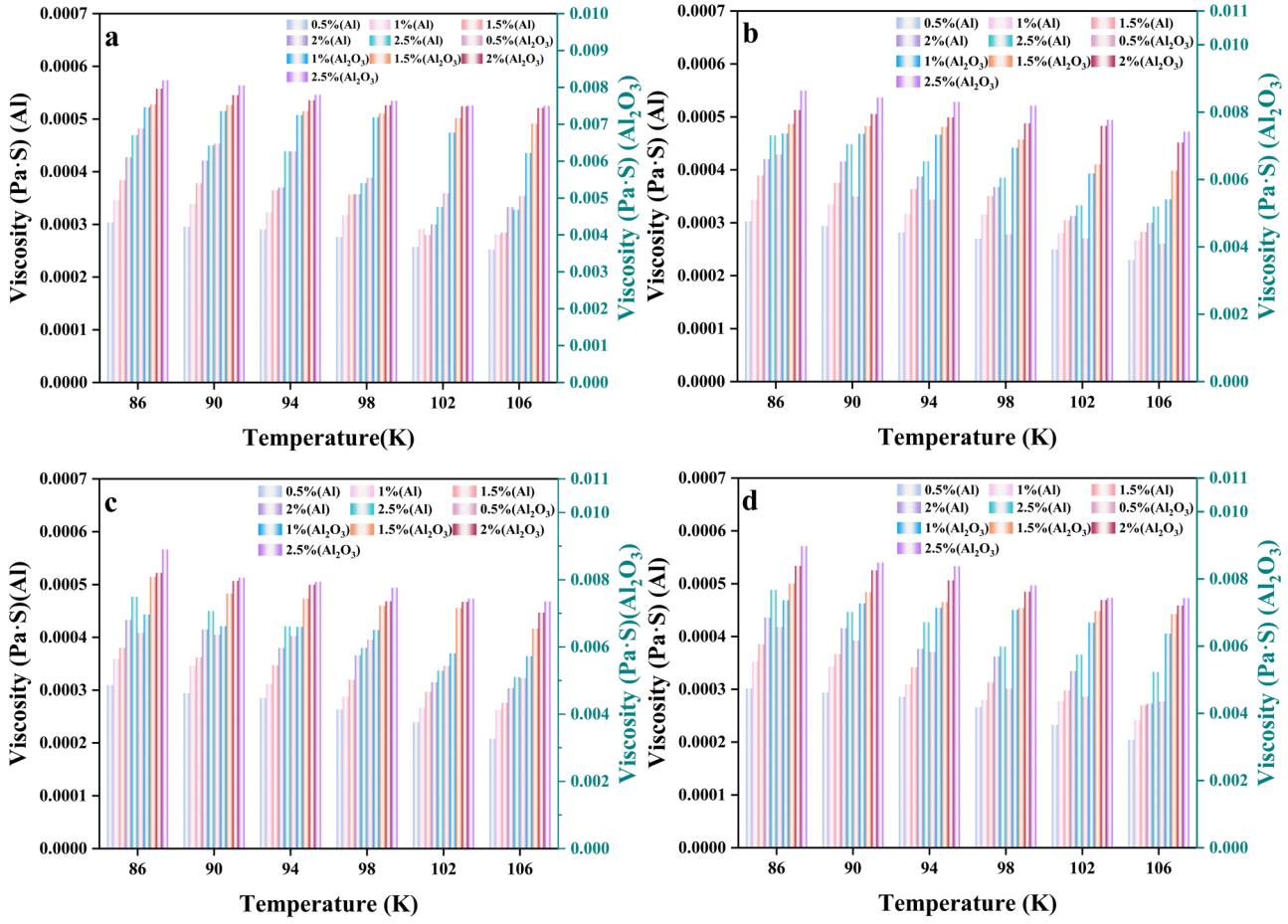

Figure 20: Differences and similarities in viscosity of Al–Ar nanofluid and Al_2O_3–Ar nanofluid with variations in volume fraction. (a) Cylinder, (b) sphere, (c) cube, and (d) platelets.

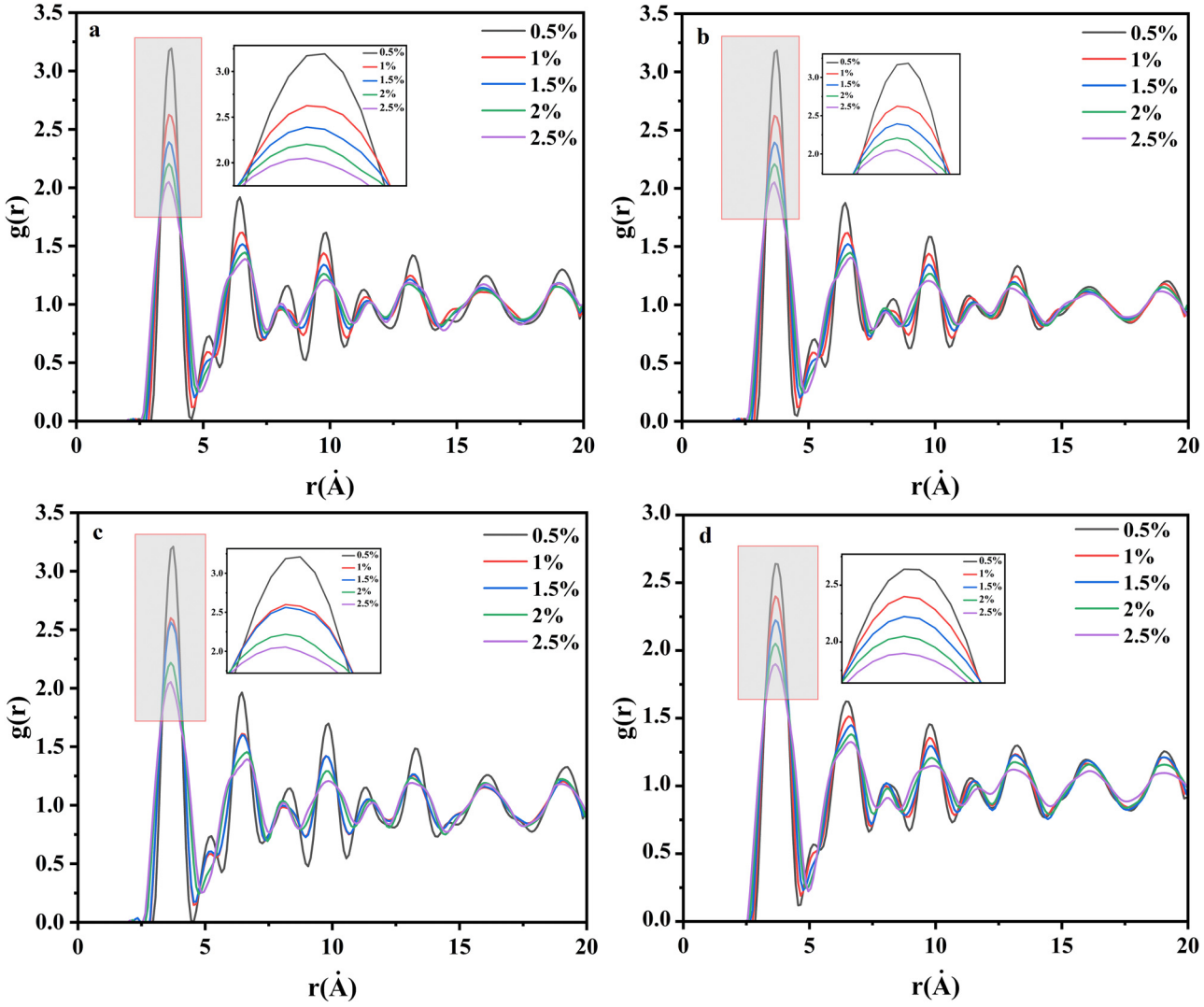

Figure 21: RDF curves of Al–Ar nanofluid with different shapes of NPs at various volume fractions when the temperature is 86 K. (a) 86 K cylinder, (b) 86 K sphere, (c) 86 K cube, and (d) 86 K platelets.

3.7 RDF study of Al–Ar nanofluid and Al_2O_3–Ar nanofluid

In order to further analyze the thermal conductivity and viscosity of Al–Ar nanofluid and Al_2O_3–Ar nanofluid from a microscopic perspective, and to understand the internal mechanisms related to temperature, NP shape, and volume fraction variations, as well as to compare the similarities and differences revealed by their microscopic structures, we computed the RDF for both Al–Ar nanofluid and Al_2O_3–Ar nanofluid [54]. The molecular dynamics simulation environment employed in the previous sections, dedicated to studying thermal conductivity, was utilized to derive the necessary data for RDF calculations.

The same setup we used before to simulate how heat moves through materials was also used to gather the information we needed for calculating RDF.

Figures 21 and 22 show us the curves that represent how atoms are arranged in the Al–Ar nanofluid and Al_2O_3–Ar nanofluid when we use NPs of different shapes. We can see how these curves change as we add more NPs to the fluid in both cases. First, there are noticeable differences in the RDF curves of NPs with different shapes in both nanofluids. However, the overall trends are consistent: the RDF curves of both Al–Ar nanofluid and Al_2O_3–Ar nanofluid reach their peaks at an NP volume fraction of 0.5%. As the volume fraction decreases, the peaks gradually shift to the left and decrease in magnitude. Additionally, in Figures 21

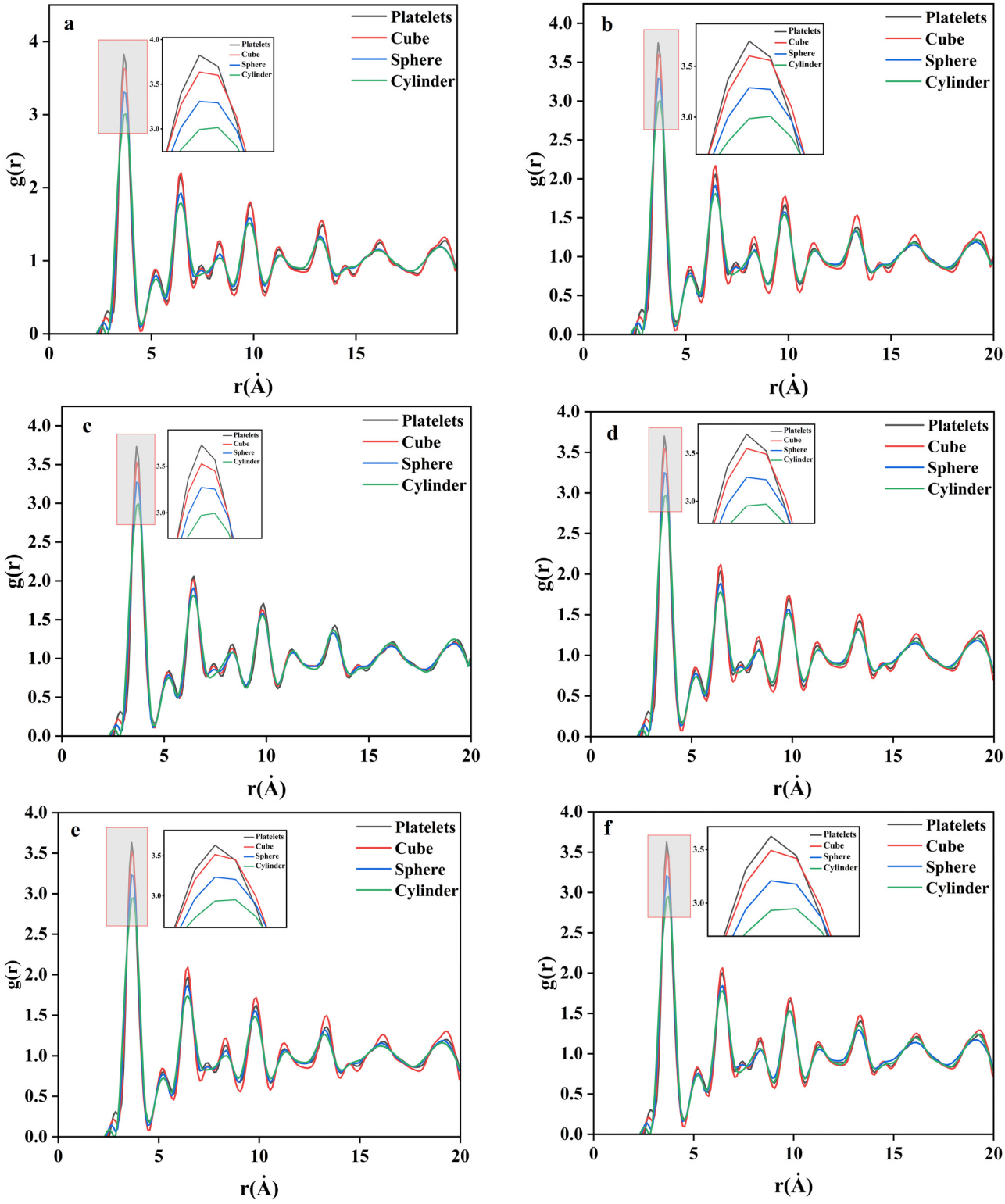

Figure 22: RDF curves of Al_2O_3–Ar nanofluid with different shapes of NPs at 86 K under various volume fractions.(a) 2% 86 K, (b) 2% 90 K, (c) 2% 94 K, (d) 2% 98 K, (e) 2% 102 K, and (f) 2% 106 K.

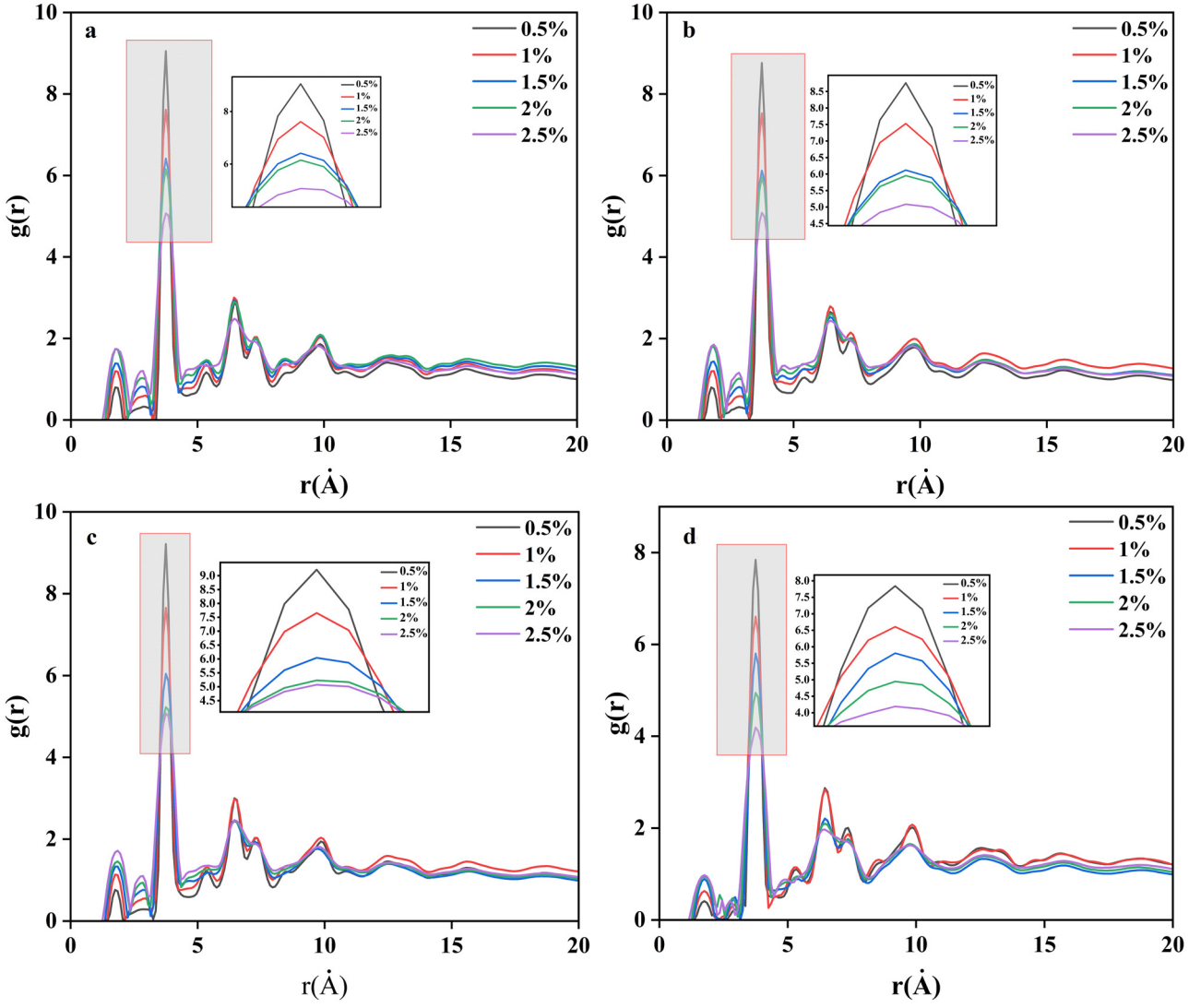

Figure 23: RDF curves of Al–Ar nanofluid with different shapes of NPs at a volume fraction of 2% under various temperatures. (a) 86 K cylinder, (b) 86 K sphere, (c) 86 K cube, and (d) 86 K platelets.

and 23, the RDF curve in (d) is more uniform than the curves in (a), (b), and (c). This indicates that nanofluids containing NPs with higher *S*/*V* values exhibit a more balanced density change in the internal solid–liquid interface layer, demonstrating excellent research and experimental properties. Furthermore, we observe that the peak positions of the RDF curves in Al–Ar nanofluid are more evenly distributed. This suggests that the microstructure of Al–Ar nanofluid (metal nanofluid) exhibits more "short-range order and long-range disorder" liquid characteristics and "long-range order" solid characteristics compared to Al_2O_3–Ar nanofluid (metal oxide nanofluid). This explanation aligns with the research result that the thermal conductivity of Al–Ar nanofluid (metal nanofluid) is higher than that of Al_2O_3–Ar nanofluid (metal oxide nanofluid) [39].

Figures 23 and 24, respectively, illustrate the RDF curves of Al–Ar nanofluid and Al_2O_3–Ar nanofluid with different-shaped NPs at a volume fraction of 2% under varying temperatures. From the graphs, it is observed that the RDF curves of both nanofluids exhibit narrow and tall peaks at their highest points, followed by broader and flatter features in the subsequent peaks. This further indicates the formation of a uniform solid–liquid interface layer around NPs in nanofluids, facilitating the aggregation of numerous BF atoms around the NPs [70]. In this study, the RDF curve of Al_2O_3–Ar nanofluid shows a more pronounced manifestation of this feature compared to the RDF curve of Al–Ar nanofluid, signifying a greater accumulation of Ar atoms around the NPs in Al_2O_3–Ar nanofluid. This deeper interpretation aligns with the observation

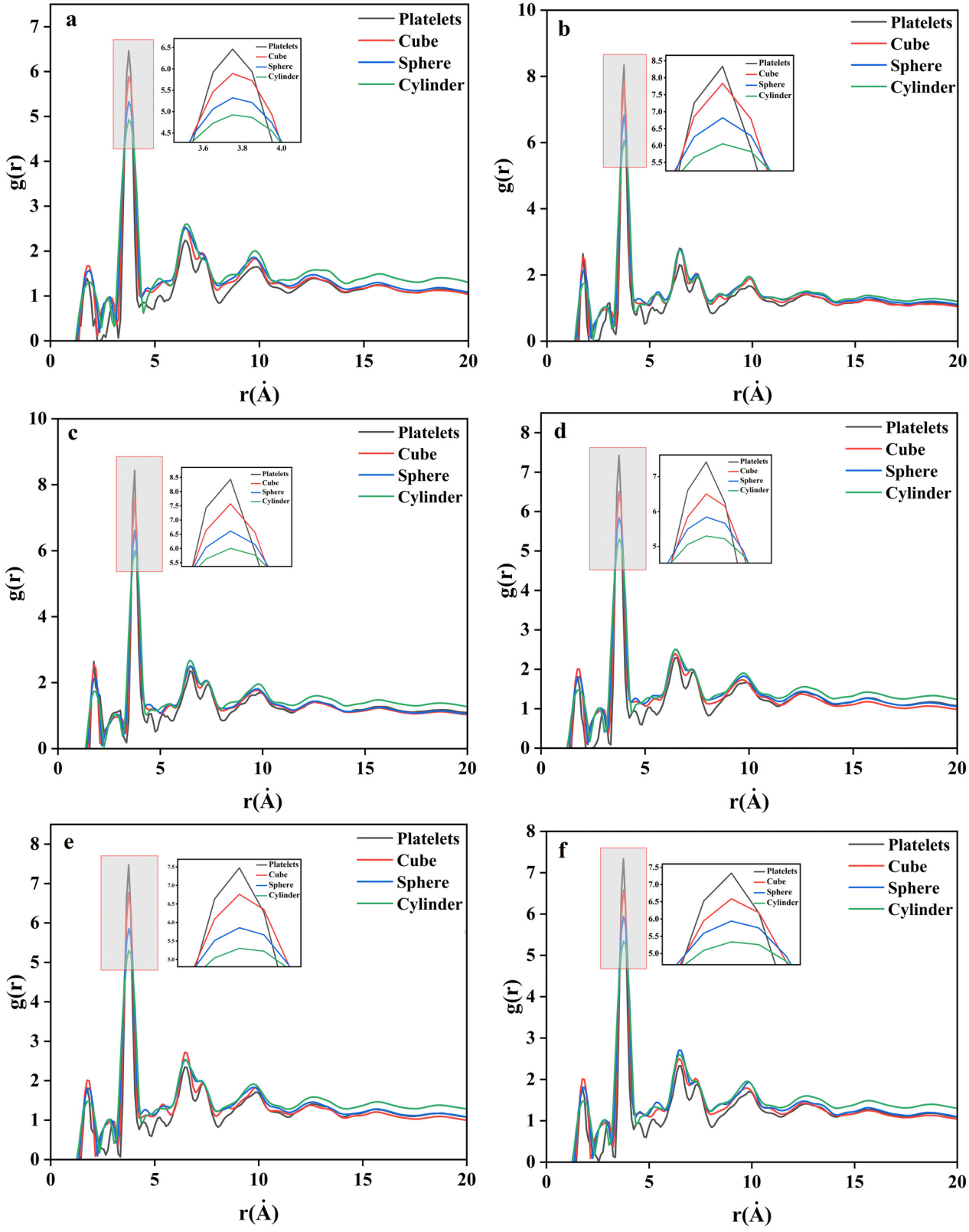

Figure 24: RDF curves of Al_2O_3–Ar nanofluid with different shapes of NPs at 2% volume fraction under various temperatures. (a) 2% 86 K, (b) 2% 90 K, (c) 2% 94 K, (d) 2% 98 K, (e) 2% 102 K, and (f) 2% 106 K.

that the viscosity of Al_2O_3–Ar nanofluid is greater than that of Al–Ar nanofluid, providing further insight into the underlying mechanisms of lower viscosity in nanofluids formed by metallic NPs compared to those formed by their metal oxide counterparts with the same BF. This is consistent with the research conducted by Chen *et al.* [70], who studied the thermal conductivity and viscosity of Cu–Ar nanofluids. By incorporating RDF curves, they explained the order of magnitude of nanofluid viscosity values. This consistency with our findings underscores the scientific validity and reliability of our results.

The peak magnitudes in both nanofluids follow the order: platelets > cube > sphere > cylinder, consistent with the decreasing sequence of S/V values for NPs of different shapes. This phenomenon further underscores the correlation between the density of the solid–liquid interface layer and the NP shape factor S/V. This observation is highly consistent with the results of Essajai *et al.* [54] and Cui *et al.* [55,56], indicating that the enhancement of thermal conductivity in nanofluids depends more on the increase in the S/V values of NPs. This is primarily attributed to the significant increase in the density of the nanolayer within nanofluids, as evident in the RDF analysis conducted in this study.

4 Conclusions

This study comprehensively investigates, for the first time at the microscopic level, the similarities and differences in the thermal–physical properties of nanofluids composed of metals and their oxides in the same type of BF. By integrating the effects of NP shape (S/V ratio), temperature, NP volume fraction, and employing research methods such as NEMD, RNEMD, RDF, and PDOS, we unveil, for the first time, the microscopic mechanisms underlying the similarities and differences in the thermal–physical properties of nanofluids composed of metals and their oxides in the same type of BF.

The research findings indicate that the thermal conductivity of Al_2O_3–Ar nanofluids and Al–Ar nanofluids both generally increases with rising temperature, NP volume fraction, and NP S/V ratio. However, under identical conditions of temperature, NP volume fraction, and shape, the thermal conductivity of Al–Ar nanofluids is higher than that of Al_2O_3–Ar nanofluids. Regarding viscosity, the overall trend for both Al_2O_3–Ar nanofluids and Al–Ar nanofluids is a decrease with increasing temperature and an increase with increasing NP volume fraction, with minimal influence from the S/V ratio. However, under identical conditions of temperature, NP volume fraction, and shape, the viscosity of Al_2O_3–Ar nanofluids is higher than that of Al–Ar nanofluids.

In response to the observed phenomena regarding the thermal conductivity of the nanofluids mentioned earlier, this study reveals the underlying mechanisms at the microscopic level. We investigated the PDOS of Al, Ar, and Al_2O_3 in nanofluids under different temperature conditions, NP volume fractions, and NP shapes. The results indicate that the percentage overlap of PDOS curves between Al and Ar is as follows: Group 1: 99.991%, Group 2: 99.98%, Group 3: 99.976%, Group 4: 99.991%, Group 5: 99.99%, Group 6: 99.995%. The percentage overlap of PDOS curves between Al_2O_3 and Ar is as follows: Group 1: 99.313%, Group 2: 99.847%, Group 3: 98.477%, Group 4: 99.406%, Group 5: 98.641%, Group 6: 99.837%. Overall, the percentage overlap of PDOS curves between Al and Ar is higher than that between Al_2O_3 and Ar, suggesting that the phonon transport at the microscopic level and interfacial thermal conductance explains the obtained results where the thermal conductivity of Al–Ar nanofluids is higher than that of Al_2O_3–Ar nanofluids. This study also elucidates, for the first time, the microscopic mechanisms underlying the similarities and differences in thermal conductivity of nanofluids composed of metals and their oxides.

Furthermore, we compared the RDF curves of Al–Ar nanofluids and Al_2O_3–Ar nanofluids under constant temperature conditions, considering different NP shapes and volume fractions. The study reveals that the RDF curve peaks in Al–Ar nanofluids are more evenly distributed, indicating that the microstructure of Al–Ar nanofluids (metal nanofluids) exhibits more characteristics of "short-range order and long-range disorder" typical of liquids, as well as "long-range order" characteristics typical of solids, compared to Al_2O_3–Ar nanofluids (metal oxide nanofluids). This finding also explains why the thermal conductivity of Al–Ar nanofluids is higher than that of Al_2O_3–Ar nanofluids, providing novel insights into the microscopic mechanisms underlying the similarities and differences in the thermal conductivity of nanofluids composed of metals and their oxides.

Regarding the observed phenomena of viscosity in the aforementioned nanofluids, this study delves into the internal mechanisms from a microscopic structural perspective. We compared the RDF curves of Al–Ar nanofluids and Al_2O_3–Ar nanofluids under different temperature conditions, NP volume fractions, and shapes. The study reveals that the RDF curve of Al_2O_3–Ar nanofluids exhibits narrower and higher peak features, followed by broader and flatter subsequent peaks, compared to the RDF curve of Al–Ar nanofluids. This suggests that in Al_2O_3–Ar nanofluids, a more uniform solid–liquid interface layer forms around the

NPs, attracting more Ar atoms. This deeper understanding elucidates why the viscosity of Al_2O_3–Ar nanofluids is greater than that of Al–Ar nanofluids and provides unprecedented insights into the microscopic mechanisms underlying the similarities and differences in the viscosity of nanofluids composed of metals and their oxides.

This study, starting from factors such as temperature, NP shape (S/V ratio), and NP volume fraction, investigates for the first time the similarities and differences in the thermal–physical properties of nanofluids composed of metals and their oxides, represented by Al_2O_3–Ar nanofluids and Al–Ar nanofluids. In future research, we plan to extend these findings to a broader range of nanofluids and employ additional methods to analyze from a microscopic perspective. Our goal is to develop universal conclusions about the thermal conductivity of nanofluids composed of metals and their oxides in the same type of BF, providing guidance for the selection and application of nanofluids in industrial settings.

The findings of this study have significant implications for the selection of nanofluids in specific engineering applications. For instance, in the field of thermal management of electronic devices, maximizing the cooling efficiency of electronic chips is crucial. This requires the cooling medium in microchannels to have excellent thermal conductivity and other thermal properties. Nanofluids are ideal cooling media, but selecting the most cost-effective type of nanofluid is a challenge. Our comparative study on the thermal properties of nanofluids composed of metals and metal oxides with the same BF provides valuable guidance. For applications in electronic device thermal management, where high thermal conductivity and superior physical properties are needed, metal NP-based nanofluids can be directly chosen over metal oxide NP-based nanofluids. Conversely, for engineering applications that require a higher viscosity fluid medium, metal oxide NP-based nanofluids can be selected. This research provides important theoretical and practical guidance for the selection of nanofluids in engineering applications.

Similarly, in the fields of battery design and prevention of thermal runaway, temperature management of batteries is a critical area. Many researchers incorporate nanofluids into battery designs to prevent thermal runaway. However, determining the most suitable nanofluid for battery thermal management is a challenging question. Our study on the differences in thermal properties between nanofluids formed by metal NPs and metal oxide NPs can provide guidance on the integration of thermal conductivity, viscosity, and other thermal properties into battery thermal management. When selecting a nanofluid as the cooling medium for battery thermal management, our research can guide the choice of nanofluid type that offers optimal cooling performance. Additionally, our research can help researchers select appropriate NP shapes and volume fraction parameters. Furthermore, our study can assist researchers in choosing nanofluids with higher thermal conductivity from those formed by metal and metal oxide NPs for use as cooling media in battery thermal management.

Overall, our research provides highly valuable guidance on the selection of nanofluids for engineering applications. We have conducted a detailed microlevel analysis of the differences in thermal properties between nanofluids composed of metal NPs and those composed of metal oxide NPs. This analysis reveals the internal mechanisms underlying these differences. Our findings hold significant research and practical implications in the fields of nanofluid research and engineering, offering crucial insights for both theoretical studies and real-world applications.

This study investigates the differences in thermophysical properties and internal microscopic mechanisms of nanofluids when the NPs are metal *versus* metal oxide. Serving as a preliminary research topic for the selection of cooling fluids in electronic chip thermal management, this study utilized Ar-based nanofluids, which offer relatively convenient simulation conditions. In our future research, we plan to extend our conclusions to the thermophysical properties of water-based nanofluids containing metal and metal oxide NPs. This will allow us to derive general conclusions applicable to various nanofluids, providing theoretical and practical guidance for selecting nanofluid types in engineering applications requiring nanofluids as heat transfer media.

As previously mentioned, this study offers both theoretical and practical guidance for selecting cooling fluids in electronic chip thermal management. Additionally, it can provide guidance for all engineering applications aiming to enhance heat transfer using nanofluids, such as battery design and prevention of thermal runaway, microchannel heat exchange, photothermal conversion, and energy storage. This research holds significant theoretical significance for the practical application of nanofluids, offering convenience and indispensable guidance for their use in real-world applications.

Furthermore, it explains the internal mechanisms underlying the discovered patterns from a microscopic structural perspective. This research extends the study of thermal properties of nanofluids and provides valuable insights into the investigation of nanofluids composed of metals and their oxides with the same base liquid, thereby offering guidance for further research in this field. Moreover, it holds significant implications for the study of the microscopic mechanisms of nanofluids.

Funding information: This research was financially supported by National Natural Science Foundation of China under Contract (No. 52069010 and No. 51966005) is gratefully acknowledged.

Author contributions: Chenghang Li: conceptualization, data curation, investigation, methodology, project administration, resources, software, supervision, validation, visualization, writing – original draft, writing – review and editing. Zhumei Lu: resources, validation. Shan Qing: funding acquisition, methodology. Haoming Huang: validation. Xiaohui Zhang: funding acquisition, methodology. All authors have accepted responsibility for the entire content of this manuscript and approved its submission.

Conflict of interest: The authors state no conflict of interest.

References

[1] Sajid MU, Ali HM. Thermal conductivity of hybrid nanofluids: a critical review. Int J Heat Mass Transf. 2018;126:211–34.
[2] Qiu L, Zhu N, Feng Y, Michaelides EE, Żyła G, Jing D, et al. A review of recent advances in thermophysical properties at the nanoscale: from solid state to colloids. Phys Rep. 2020;843:1–81.
[3] Khodadadi H, Aghakhani S, Majd H, Kalbasi R, Wongwises S, Afrand M. A comprehensive review on rheological behavior of mono and hybrid nanofluids: effective parameters and predictive correlations. Int J Heat Mass Transf. 2018;127:997–1012.
[4] Yang L, Du K. A comprehensive review on heat transfer characteristics of TiO_2 nanofluids. Int J Heat Mass Transf. 2017;108:11–31.
[5] Lomascolo M, Colangelo G, Milanese M, Risi AD. Review of heat transfer in nanofluids: Conductive, convective and radiative experimental results. Renewable Sustainable Energy Rev. 2015;43:1182–98.
[6] Ioaa B, Maar A, Za A, Yy A, Tas C. Application of support vector regression and artificial neural network for prediction of specific heat capacity of aqueous nanofluids of copper oxide – ScienceDirect. Sol Energy. 2020;197:485–90.
[7] Maxwell JC. A treatise on electricity and magnetism. Spat Spatiotemporal Epidemiol. 2010;1:231–7.
[8] Mashali F, Languri EM, Davidson J, Kerns D, Johnson W, Nawaz K, et al. Thermo-physical properties of diamond nanofluids: A review. Int J Heat Mass Transf. 2018;129:1123–35.
[9] Alawi AO, Sidik NAC, Xian HW, Kean TH, Kazi NS. Thermal conductivity and viscosity models of metallic oxides nanofluids. Int J Heat Mass Transf. 2018;116:1314–25.
[10] Minakov AV, Pryazhnikov MI, Guzei DV. Rudyak. Thermal conductivity measurements of nanofluids. Int J Heat Mass Transf. 2017;104:1275–82.
[11] Kanti PK, Sharma P, Sharma KV, Maiya MP. The effect of pH on stability and thermal performance of graphene oxide and copper oxide hybrid nanofluids for heat transfer applications: Application of novel machine learning technique. J Energy Chem. 2023;82:359–74.
[12] Toghraie D, Hekmatifar M, Salehipour Y, Afrand M. Molecular dynamics simulation of Couette and Poiseuille Water-Copper nanofluid flows in rough and smooth nanochannels with different roughness configurations. Chem Phys. 2019;527:110505.
[13] Kanti P, Sharma KV, Ramachandra CG, Panitapu B. Stability and thermophysical properties of fly ash nanofluid for heat transfer applications. Heat Transf. 2020;49(8):4722–37.
[14] Agarwal R, Verma K, Agrawal NK, Singh R. Sensitivity of thermal conductivity for Al_2O_3 nanofluids. Exp Therm Fluid Sci. 2017;80:19–26.
[15] Shinde SM, Patil PA, Bhojwani VK. An experimental study to investigate the dynamic behaviour of thermal conductivity for different concentrations of Al_2O_3 nanofluid. Int J Ambient Energy. 2020;41:1321–6.
[16] Kanti PK, Sharma P, Maiya MP, Sharma KV. The stability and thermophysical properties of Al_2O_3-graphene oxide hybrid nanofluids for solar energy applications: Application of robust autoregressive modern machine learning technique. Sol Energy Mater Sol Cell. 2023;253:112207.
[17] Topal I, Servantie J. Molecular dynamics study of the thermal conductivity in nanofluids. Chem Phys. 2018;516:147–51.
[18] Hamid KA, Azmi WH, Nabil MF, Mamat R, Sharma KV. Experimental investigation of thermal conductivity and dynamic viscosity on nanoparticle mixture ratios of TiO_2-SiO_2 nanofluids. Int J Heat Mass Tran. 2018;116:1143–52.
[19] Daviran S, Kasaeian A, Tahmooressi H, Rashidi A, Wen DS, Mahian O. Evaluation of clustering role versus Brownian motion effect on the heat conduction in nanofluids: a novel approach. Int J Heat Mass Transf. 2017;108:822–9.
[20] Lee SL, Saidur R, Sabri MFM, Min TK. Molecular dynamic simulation on the thermal conductivity of nanofluids in aggregated and non-aggregated states. Numer Heat Transfer, Part. 2015;68(4):432–53.
[21] Zerradi H, Mizani S, Loulijat H, Dezairi A, Ouaskit S. Population balance equation model to predict the effects of aggregation kinetics on the thermal conductivity of nanofluids. J Mol Liq. 2016;218:373–83.
[22] Hong JG, Kim D. Effects of aggregation on the thermal conductivity of alumina/water nanofluids. Thermochim Acta. 2012;542:28–32.
[23] Wang RJ, Qian S, Zhang ZQ. Investigation of the aggregation morphology of nanoparticle on the thermal conductivity of nanofluid by molecular dynamics simulations. Int J Heat Mass Transf. 2018;127:1138–46.
[24] Kang HB, Zhang YW, Yang M, Li L. Molecular dynamics simulation on effect of nanoparticle aggregation on transport properties of a nanofluid. J Nanotechnol Eng Med. 2012;3(2):021001.
[25] Guo HB, Zhao NB. Interfacial layer simulation and effect on Cu-Ar nanofluids thermal conductivity using molecular dynamics method. J Mol Liq. 2018;259:40–7.
[26] Zhou L, Zhu J, Ma H. One-step synthesis of Cu/Therminol VP-1 nanofluids by phase transfer method and their thermal stability and thermophysical properties. J Nanopart Res. 2024;26(2):35.
[27] Ganesan V, Louis C, Damodaran SP. Novel nanofluids based on magnetite nanoclusters and investigation on their cluster size-dependent thermal conductivity. J Phys Chem C. 2018;122(12):6918–29.
[28] Feng Y, Yu B, Xu P, Zou M. The effective thermal conductivity of nanofluids based on the nanolayer and the aggregation of nanoparticles. J Phys D Appl Phys. 2007;40(10):3164–71.
[29] Thajudeen T, Hogan CJ. Forced and natural convection in aggregate-laden nanofluids. J Nanopart Res. 2011;13(12):7099–113.

[30] Main K, Eberl B, Mcdaniel D, Tikadar A, Paul TC, Khan JA. Nanoparticles shape effect on viscosity and thermal conductivity of ionic liquids based nanofluids. In Proceedings of the 5th Thermal and Fluids Engineering Conference (TFEC). New Orleans, LA, USA; April 2020. p. 5–8.
[31] Zhang R, Zhang X, Qing S, Luo Z, Liu Y. Investigation of nanoparticles shape that influence the thermal conductivity and viscosity in argon-based nanofluids: A molecular dynamics simulation. Int J Heat Mass Transf. 2023;207:124031.
[32] Zhu D, Wang L, Yu W, Xie H. Intriguingly high thermal conductivity increment for CuO nanowires contained nanofluids with low viscosity. Sci Rep. 2018;8:5282.
[33] Kanti P, Sharma KV, Raja Sekhar Y. Influence of particle size on thermal conductivity and dynamic viscosity of water-based Indian coal fly ash nanofluid. Heat Transf. 2022;51(1):413–33.
[34] Maheshwary P, Handa C, Nemade K, Chaudhary S. Role of nanoparticle shape in enhancing the thermal conductivity of nanofluids. Mater Today: Proc. 2020;28:873–8.
[35] Wang R, Feng C, Zhang Z, Shao C, Du J. What quantity of charge on the nanoparticle can result in a hybrid morphology of the nanofluid and a higher thermal conductivity? Powder Technol. 2023;422:118443.
[36] Jin X, Guan H, Wang R, Huang L, Shao C. The most crucial factor on the thermal conductivity of metal-water nanofluids: match degree of the phonon density of state. Powder Technol. 2022;412:117–969.
[37] Wang X, Jing D. Determination of thermal conductivity of interfacial layer in nanofluids by equilibrium molecular dynamics simulation. Int J Heat MassTransf. 2019;128:199–207.
[38] Zhou L, Zhu J, Zhao Y, Ma H. A molecular dynamics study on thermal conductivity enhancement mechanism of nanofluids –effect of nanoparticle aggregation. Int J Heat Mass Transf. 2021;183:122–4.
[39] Kang H, Zhang Y, Yang M. Molecular dynamics simulation of thermal conductivity Of Cu€“Ar nanofluid using EAM potential for Cu€”Cu interactions. Appl Phys A Mater Sci Process. 2011;103:1001–8.
[40] Daw MS, Baskes MI. Embedded-atom method: derivation and application to impurities, surfaces, and other defects in metals. Phys Rev B Condens Matter. 1984;29(12):6443–53.
[41] Liao J, Zhang A, Qing S, Zhang X, Luo Z. Investigation on the aggregation structure of nanoparticle on the thermal conductivity of nanofluids by molecular dynamic simulations. Powder Technol. 2022;395:584–91.
[42] Kang H, Zhang Y, Yang M. Molecular dynamics simulation of thermal conductivity of Cu-Ar nanofluid using EAM potential for Cu-Cu interactions. Appl Phys A. 2011;103(4):1001–8.
[43] Zeroual S, Loulijat H, Achehal E, Estellé P, Hasnaoui A, Ouaskit S. Viscosity of Ar-Cu nanofluids by molecular dynamics simulations: effects of nanoparticle content, temperature and potential interaction. J Mol Liq. 2018;268:490–6.
[44] Stukowski A. Visualization and analysis of atomistic simulation data with OVITO–the open visualization tool. Model Simul Mater Sci Eng. 2009;18:015012.
[45] Zoli L, Sciti D, Sani E. Zirconium diboride-based nanofluids for solar energy applications. J Mol Liq. 2021;322:114–981.
[46] Carrillo-Berdugo I, Grau-Crespo R, Zorrilla D, Navas J. Interfacial molecular layering enhances specific heat of nanofluids: evidence from molecular dynamics. J Mol Liq. 2021;325:115–217.
[47] Müller-Plathe F. Reversing the perturbation in nonequilibrium molecular dynamics: an easy way to calculate the shear viscosity of fluids. Phys Rev E. 1999;59:4894.
[48] Fernandez GA, Vrabec J, Hasse H. A molecular simulation study of shear and bulk viscosity and thermal conductivity of simple real fluids. Fluid Phase Equilib. 2009;221:157–63.
[49] Rostami S, Zarringhalam M, Alizadeh A, Toghraie D, Goldanlou AS. Molecular dynamic simulation of Argon boiling flow inside smooth and rough microchannels by considering the effects of cubic barriers. J Mol Liq. 2020;312:113130.
[50] Kanhaiya K, Kim S, Im W, Heinz H. Accurate simulation of surfaces and inter-faces of ten FCC metals and steel using Lennard–Jones potentials. npj Comput Mater. 2021;7:17.
[51] Liu J, Lu WQ. Molecular dynamics simulation of the thermal conductivity of Al-Ar nanofluid using simplified model. ASME Micro/Nanoscale Heat and Mass Transfer International Conference. Shanghai, Peoples R China: 2009.
[52] Darvanjooghi MHK, Esfahany MN. Experimental investigation of the effect of nanoparticle size on thermal conductivity of in-situ prepared silica–ethanol nano-fluid. Int Commun Heat Mass Transf. 2016;77:148–54.
[53] Koo J, Kleinstreuer C. A new thermal conductivity model for nanofluids. J Nanopart Res. 2004;6(6):577–88.
[54] Essajai R, Mzerd A, Hassanain N, Qjani M. Thermal conductivity enhance-ment of nanofluids composed of rod-shaped gold nanoparticles: insights from molecular dynamics. J Mol Liq. 2019;293:111494.
[55] Maheshwary PB, Handa CC, Nemade KR. A comprehensive study of effect of concentration, particle size and particle shape on thermal conductivity of titania/water based nanofluid. Appl Therm Eng. 2017;119:79–88.
[56] Cui W, Shen Z, Yang J, Wu S, Bai M. Influence of nanoparticle properties on the thermal conductivity of nanofluids by molecular dynamics simulation. RSC Adv. 2014;4:161–92.
[57] Lee SW, Park SD, Kang S, Bang IC, Kim JH. Investigation of viscosity and thermal conductivity of SiC nanofluids for heat transfer applications. Int J Heat Mass Transf. 2011;54(1–3):433–8.
[58] Masoumi N, Sohrabi N, Behzadmehr A. A new model for calculating the effective viscosity of nanofluids. J Phys D Appl Phys. 2009;42(5):055501.
[59] Ranjbarzadeh R, Akhgar A, Musivand S, Afrand M. Effects of graphene oxide silicon oxide hybrid nanomaterials on rheological behavior of water at various time durations and temperatures: Synthesis, preparation and stability. Powder Technol. 2018;335:375–87.
[60] Fujiwara K, Daimo M, Ueki Y, Ohara T, Shibahara M. Thermal conductivity of nanofluids: a comparison of EMD and NEMD calculations. Int J Heat Mass Transf. 2019;144:118695.
[61] Song HL, Dong KP, Kang DB. Molecular dynamics simulations for transport coefficients of liquid argon: new approaches. Korean Chem Soc. 2003;24(2):178–82.
[62] Essajai R, Rachadi A, Feddi E, Hassanain N. MD simulation-based study on the thermodynamic, structural and liquid properties of gold nanostructures. Mater Chem Phys. 2018;5:045–121.
[63] Kole M, Dey TK. Enhanced thermophysical properties of copper nanoparticles dispersed in gear oil. Appl Therm Eng. 2013;56:45–53.
[64] Milanese M, Iacobazzi F, Colangelo G, de Risi A. An investigation of layering phenomenon at the liquid-solid interface in Cu and CuO based nanofluids. Int J Heat Mass Transf. 2016;103:564–71.
[65] Jamal-Abad MT, Zamzamian A, Dehghan M. Experimental studies on the heat transfer and pressure drop characteristics of Cu-water

and Al-water nanofluids in a spiral coil. Exp Therm Fluid Sci. 2013;47:206–12.
[66] Ruvo TH, Shuvo MS, Saha S. Revisiting thermo-physical property models of Al2O3-Water nanofluid for natural convective flow. Heliyon. 2024;10(5):e26964.
[67] El Hadoui B, Kaddiri M. Double diffusive natural convection with variable properties of nanofluid using lattice Boltzmann method. Int Days Therm Sci Energy. 2024;22–32.
[68] Huang H, Li C, Huang S, Shang Y. A sensitivity analysis on thermal conductivity of Al2O3-H2O nanofluid: A case based on molecular dynamics and support vector regression method. J Mol Liq. 2024;393:123652.
[69] Xue GB, Zhong J, Gao S, Wang B. Correlation between the free volume and thermal conductivity of porous poly(vinyl alcohol)/reduced graphene oxide composites studied by positron spectroscopy. Carbon. 2016;96:871–8.
[70] Chen J, Han K, Wang S, Liu X, Wang P, Chen J. Investigation of enhanced thermal properties of CuAr nanofluids by reverse non equilibrium molecular dynamics method. Powder Technol. 2019;356:559–65.